BlurGuard: A Simple Approach for Robustifying Image Protection Against AI-Powered Editing

Jinsu Kim^{1*} Yunhun Nam^{1*} Minseon Kim² Sangpil Kim¹ Jongheon Jeong¹

¹Korea University ²Microsoft Research Montréal

*{tonmmy222, yh0326}@korea.ac.kr

Abstract

Recent advances in text-to-image models have increased the exposure of powerful image editing techniques as a tool, raising concerns about their potential for malicious use. An emerging line of research to address such threats focuses on implanting ("protective") adversarial noise into images before their public release, so future attempts to edit them using text-to-image models can be impeded. However, subsequent works have shown that these adversarial noises are often easily "reversed," e.g., with techniques as simple as JPEG compression, casting doubt on the practicality of the approach. In this paper, we argue that adversarial noise for image protection should not only be imperceptible, as has been a primary focus of prior work, but also *irreversible*, viz., it should be difficult to detect as noise provided that the original image is hidden. We propose a surprisingly simple method to enhance the robustness of image protection methods against noise reversal techniques. Specifically, it applies an adaptive per-region Gaussian blur on the noise to adjust the overall frequency spectrum. Through extensive experiments, we show that our method consistently improves the per-sample worst-case protection performance of existing methods against a wide range of reversal techniques on diverse image editing scenarios, while also reducing quality degradation due to noise in terms of perceptual metrics. Code is available at https://github.com/jsu-kim/BlurGuard.

1 Introduction

Generative AI has been revolutionizing computer vision with its remarkable capabilities in visual synthesis across complex domains, including images [4, 37, 67], 3D models [16, 52, 70], and videos [8, 69]. *Text-to-image models* [23, 67, 75], powered by large-scale diffusion-based generative models [33, 73, 85], are one of the representative examples of current generative AI, given the significant interest they have garnered within the research community. For example, these models have facilitated diverse application research, *e.g.*, personalizing the models into specific artistic styles [26, 74], inpainting or editing an image based on textual prompts [55, 58], and even following detailed instructions [7], to name a few. Publicly available text-to-image models, such as Stable Diffusion (SD) [23, 67], have further expanded the accessibility of these techniques to broader audiences.

Despite advancements, the broader accessibility of text-to-image models has also raised serious concerns about their potential for misuse. Specifically, natural-looking manipulation of an image can produce harmful or deceptive content, resulting in fake news, violations of copyright, publicity or even portrait rights. For instance, current models can easily replicate an artist's style without permission or infringe on portrait rights by manipulating images of any victims. Such malicious editing is particularly concerning as the quality of image generation approaches a level that is nearly indistinguishable from reality; this "realism" of generative AI increases the risks of misinformation,

^{*}Equal contribution.

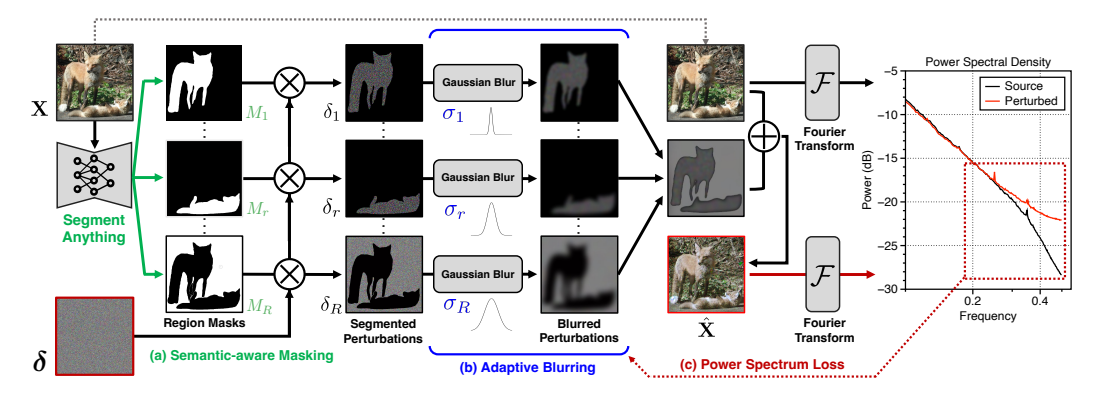


Figure 1: Overview of *BlurGuard*, a novel framework for constructing robust image protection. We (a) leverage Segment Anything [40] to obtain semantic-aware region-wise perturbations, (b) apply different levels of Gaussian blur, and (c) update blur-intensity parameters to minimize the power-spectrum gap before and after adding the perturbation.

harassment, intellectual property theft, and privacy violations, as manipulated images can spread false narratives, damage reputations, or exploit individuals without consent.

To mitigate these risks, recent efforts [77, 80, 90, 101] have focused on developing technical strategies to raise the cost of malicious image editing, which has been significantly lowered by generative AI. One of the prominent ideas in this direction is to apply *adversarial noise* [29, 87] to images before they are exposed to potential malicious uses [48, 49, 77, 96], ensuring that the noise is (a) imperceptible enough to preserve the original quality of the given image, and (b) capable of completely disrupting the behavior of generative AI. For example, Salman et al. [77] have shown that such noise can effectively prevent an image from being edited using off-the-shelf text-to-image models, such as Stable Diffusion.

However, later studies [34, 102] have raised concerns about the reliability of adversarial attack-based protection methods for practical use. Specifically, they found that all the existing methods are vulnerable to simple noise removal techniques, such as JPEG compression [91] and diffusion-based noise purification [63, 66], effectively neutralizing the protections and allowing attackers to bypass them. In other words, adversarial image protection is often easily "reversible." These observations suggest that *simply finding imperceptible noise is not sufficient* for withstanding diverse noise removal techniques. This is intuitively reasonable, as imperceptibility is defined by human perception, whereas existing noise removal methods are not necessarily designed to align with humans.

Contributions In this paper, we move away from the previous focus on imperceptibility as the primary criterion of crafting adversarial noise. Instead, we argue that adversarial noise should also minimally affect the original distribution of images across different representations, ensuring that it remains undetectable by detectors based on unforeseen image representations. We start by observing that adversarial attacks optimized for imperceptibility, *e.g.*, by constraining the noise within a small ℓ_{∞} -ball, often produce noise that becomes easily detectable when viewed in the frequency spectrum. We develop this observation and show that existing adversarial attack methods for image protection commonly suffer from this issue, explaining why they can be easily bypassed.

To further support our claim, we propose a surprisingly simple method that improves the robustness of adversarial attacks against noise removal by minimizing their detectability in the frequency domain. Specifically, we introduce (a) a learnable Gaussian blurring layer to effectively limit the frequency bands of adversarial noise for each semantic region of a given image, and (b) a novel objective to optimize the blurring parameters based on the power spectrum of the perturbed image (see Figure 1). In this way, the adversarial noise can automatically adjust its frequency bands to maintain high naturalness to withstand purification techniques.

We perform an extensive evaluation of our method in comparison to existing adversarial attack based image protection methods [48, 49, 77, 96], under a challenging scenario where a malicious user selects the best-case performance after diverse state-of-the-art noise removal techniques [34, 63, 102]. As an attempt to standardize the evaluation, we also construct a new curated dataset for assessing the performance of image protection techniques against malicious editing, addressing the current lack of

a public benchmark. Our results show that the proposed method, despite its simplicity, significantly improves the per-sample worst-case protection performance on the benchmark, while effectively controlling its imperceptibility as well. For example, our method could maintain the effectiveness in FID up to 93% after all purification tested, while the previous best does only 48%.

2 Related Work

Protecting images against generative AI The concept of embedding adversarial noise to protect images from unauthorized AI systems has been introduced in various contexts [17, 77, 79, 80, 90]. For example, Shan et al. [79] considered scenarios in which a "tracker" trains a facial recognition model using online photos of specific users, and proposed leveraging adversarial noise to disrupt model training and protect user privacy. Salman et al. [77] considered similar threats in the context of text-to-image model based image editing pipelines; Shan et al. [80] and Van Le et al. [90] have focused on a specific setup of *style mimicry*, where a malicious user further fine-tunes a text-to-image model to extract artistic styles in images; Choi et al. [18] have focused on *inpainting*, which modifies specific regions of human images. The robustness of image protection has only recently been explored [15, 92], but existing methods remain limited to handling a single type of editing task (*e.g.*, inpainting) and are tailored to naïve purification techniques such as JPEG. In this paper, we propose a simple and versatile method that generalizes across a broader range of image editing tasks, with a focus on the more challenging scenario of worst-case purification techniques.

Frequency-based adversarial examples Some early works constrained their adversarial perturbations within low-frequency bands for several reasons, including reducing computational cost [31], enhancing robustness [81], and improving imperceptibility [2, 13, 56, 59, 95]. In the context of generative diffusion models, Ahn et al. [1] have recently leveraged the frequency domain to enhance the imperceptibility of adversarial perturbation but they do not focus on the robustness of protection. In image watermarking, Liu et al. [51] have considered influence functions with frequency constraint to generate adversarial watermarks against personalized diffusion models, showing robustness against simple compression techniques such as JPEG and WebP. Some works [54, 35] considered low-frequency watermarks so that they remain decodable after editing. Beyond these works, we propose a simpler yet versatile frequency-based approach for robust image protection through a novel power spectrum regularization, targeting wider ranges of tasks and purification methods.

We provide more discussion of related work in Appendix A.1.

3 Preliminaries

Text-to-image diffusion models Diffusion models [22, 33, 84] learn a data distribution $p_{\text{data}}(\mathbf{x})$ through denoising interpolants between $p_{\text{data}}(\mathbf{x})$ and Gaussian noise. Text-to-image diffusion models [4, 73, 75] incorporate texts as external variables for conditional generation. From an architectural perspective, existing large-scale diffusion models typically employ one of two designs to handle high-resolution inputs: (a) latent diffusion models (LDMs) [73], which first map \mathbf{x} into a latent space of lower-resolution via an encoder $\mathbf{z} := \mathcal{E}(\mathbf{x})$, and (b) cascaded diffusion models [76], which first train a low-resolution pixel diffusion model, followed by progressive super-resolution modules.

Adversarial image protection In response to the emerging threats of malicious image editing enabled by generative AI, recent efforts [48, 49, 77, 96] have utilized adversarial examples [5, 12, 87] as a protection scheme of images against public generative models, *e.g.*, text-to-image diffusion models. In particular, PhotoGuard [77] proposes two different ways of disrupting the inner working of LDMs (*e.g.*, Stable Diffusion) through adversarial noise: either (a) by corrupting the encoder model within LDM ("*encoder attack*"), or (b) by making its denoising process more difficult ("*diffusion attack*"). For example, the encoder attack considers the following optimization given x:

$$\hat{\mathbf{x}}_{\text{adv}} = \underset{d(\hat{\mathbf{x}}, \mathbf{x}) \leq \epsilon}{\text{arg min }} L_{\text{enc}}(\hat{\mathbf{x}}), \text{ where } L_{\text{enc}} := ||\mathcal{E}(\hat{\mathbf{x}}) - \mathbf{z}_{\text{target}}||_2^2, \tag{1}$$

where $d(\cdot, \cdot)$ is a distance metric, and $\mathbf{z}_{\text{target}}$ is a certain target latent representation, e.g., that of a gray image. In practice, such an optimization is performed via projected gradient descent (PGD) [57], using a distance metric that allows easy projection while maintaining imperceptibility, such as ℓ_{∞} distance $d(\hat{\mathbf{x}}, \mathbf{x}) := \|\hat{\mathbf{x}} - \mathbf{x}\|_{\infty}$:

$$\hat{\mathbf{x}} \leftarrow \operatorname{Proj}_{\|\hat{\mathbf{x}} - \mathbf{x}\|_{\infty} \le \epsilon} \left(\hat{\mathbf{x}} - \gamma \cdot \operatorname{sign}(\nabla_{\hat{\mathbf{x}}} L_{enc}(\hat{\mathbf{x}})) \right), \tag{2}$$

where γ is the step-size for each update.

Adversarial purification The idea of neutralizing adversarial noise through *adversarial purification* methods has been repeatedly explored over time; examples include JPEG compression [30], GAN-based projection [78], and diffusion model-based denoising [63], among others. Yet, later works [3, 45] have shown that these approaches are often insufficient as a thorough defense mechanism. Given the "flipped" attack-defense relationship introduced by the new setup of adversarial protection, however, these purification methods have now become strong "attack" mechanisms [34, 102]; here, the key difference is that adversarial noise (intended for protection) no longer has the opportunity to adapt to future purification methods, even if there are ways to bypass individual purification schemes. Ultimately, we question: "Can a single adversarial noise be resilient to *all* possible purification methods, offering *irreversible* protection against evolving noise reversal techniques?"

4 Method

In approaching the above question, we argue that irreversible adversarial noise should have only minimal impact on the *data likelihood* of the original image, so that no specific purification method can project the noise back onto the given manifold defined by $p_{\text{data}}(\mathbf{x})$. We motivate this intuition by showing that existing adversarial protections, even when imperceptible in the pixel space, are often easily detectable when analyzed in their frequency bandwidth, and consequently by purification methods (Section 4.1). Based on this observation, we propose BlurGuard, a simple method to enhance robustness of adversarial protection by adaptively restricting the frequency bands of perturbation to align more closely with the natural frequency characteristics of the data, making the noise less distinguishable from the underlying distribution $p_{\text{data}}(\mathbf{x})$ (Section 4.2 and 4.3).

Threat model Consider a private image \mathbf{x} sampled from $p_{\text{data}}(\mathbf{x})$ (i.e., \mathbf{x} initially has a high data likelihood), which is accessible only to a protector (or "defender"). The goal of the protector is to find an adversarial example $\hat{\mathbf{x}}$ near \mathbf{x} such that unauthorized editing of $\hat{\mathbf{x}}$ using a given text-to-image diffusion model $p_{\theta}(\mathbf{x}, c)$ becomes difficult. In order to control the imperceptibility of $\hat{\mathbf{x}}$, we assume that $\hat{\mathbf{x}}$ is bounded within a certain ball $B_{\epsilon}(\mathbf{x})$ around \mathbf{x} , where its definition depends on the chosen distance metric $d(\cdot, \cdot)$:

$$B_{\epsilon}(\mathbf{x}) := \{ \mathbf{x}' : d(\mathbf{x}', \mathbf{x}) \le \epsilon \}. \tag{3}$$

There can be multiple ways for $\hat{\mathbf{x}}$ to disrupt the behavior of $p_{\theta}(\mathbf{x}, c)$, e.g., by corrupting either the encoder or denoiser within LDMs, as done in PhotoGuard. We denote the protector's adversarial objective as $L_{\text{adv}}(\hat{\mathbf{x}}; p_{\theta})$.

From the perspective of an *unauthorized editor* (or "attacker"), on the other hand, the goal is now to neutralize a given protected image $\hat{\mathbf{x}}$ by purifying the added adversarial noise, *i.e.*, to recover \mathbf{x} from $\hat{\mathbf{x}}$. Given the common information that \mathbf{x} has a high likelihood with respect to p_{data} , existing purification methods essentially leverage specific prior knowledge about p_{data} and aim to maximize $p_{\text{data}}(\hat{\mathbf{x}})$. For example, JPEG compression [91] is designed to remove less-frequent signals in natural scenes. In principle, the attacker has no restriction on the choice of purification methods to apply, as long as \mathbf{x} remains hidden. This means that, an "oracle" attacker, equipped with a close approximation of p_{data} , could even directly maximize $p_{\text{data}}(\hat{\mathbf{x}})$.

Need for "naturalistic" protection Ultimately, incorporating the attacker's capabilities, we consider the following minimax objective to find adversarial protection:

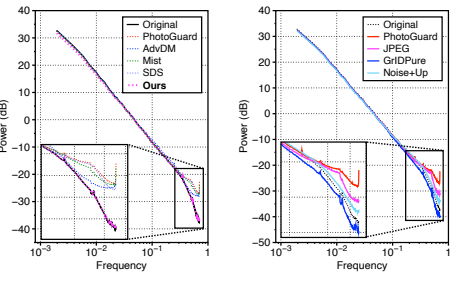
$$\hat{\mathbf{x}}_{\text{adv}} := \underset{\hat{\mathbf{x}} \in B_{\epsilon}(\mathbf{x})}{\min} \ L_{\text{adv}}(\text{purify}(\hat{\mathbf{x}}); p_{\theta}), \text{ where } \text{purify}(\hat{\mathbf{x}}) := \underset{\mathbf{y} \in B_{\epsilon}(\hat{\mathbf{x}})}{\arg \max} \ \log p_{\text{data}}(\mathbf{y}, c). \tag{4}$$

The objective (4) suggests that the optimal protection $\hat{\mathbf{x}}_{adv}$ should lie among the points in $B_{\epsilon}(\mathbf{x})$ where the data likelihood is at least $p_{\text{data}}(\mathbf{x})$; otherwise, purify($\hat{\mathbf{x}}$) could identify \mathbf{x} as a feasible point in the inner optimization, thus succeeding in reversing the protection.

4.1 A Frequency View of Adversarial Image Protection

We next question whether the existing methods for adversarial protection [49, 48, 77, 96] are capable of generating sufficiently natural perturbation, *i.e.*, ones that can effectively solve (4). In general, the

naturalness of adversarial examples has been controlled by constraining the noise to meet a certain *imperceptibility* criterion, *e.g.*, being within a small ℓ_p -ball; current adversarial protection techniques also follow this approach.



- (a) Attacked images
- (b) After purification

Figure 2: Comparisons of RAPSD on ImageNet-Edit (Appendix C.3) with SD-v1.4.

However, pursuing imperceptibility does not necessarily ensure naturalness; rather, imperceptibility is a specific instance of naturalness, when perception is limited to human vision. Given that diffusion models reconstruct images by progressively moving from low to high frequencies [72], it is natural to expect that the frequency-spectrum naturalness of an image also influences its data likelihood $p_{\rm data}$. In Figure 2, we indeed observe that an imperceptible, ℓ_{∞} -constrained image protection from various existing methods often produces a more significant deviation when viewed in its *radially-averaged power spectral density* (RAPSD), making it difficult to consider as a natural scene; *e.g.*, one that follows the $1/f^2$ -law [9].

4.2 BlurGuard: Robust Adversarial Protection via Adaptive Gaussian Blurring

Motivated by Section 4.1, we develop BlurGuard, a simple plug-and-play approach to improve the robustness of image protection methods by regularizing the power spectrum of adversarial noise. Overall, we generally observe the bias of existing image protection techniques towards high-frequency bands and aim to close this spectrum gap (from natural images) by applying "spatially-adaptive" Gaussian blur to the noise. In this way, BlurGuard can selectively allocate high-frequency noise to regions that have less impact on the overall spectrum (*e.g.*, as shown in Figure 2a), thus maintaining strong protection while appearing more natural.

Learnable Gaussian blurring To effectively control the frequency spectrum of image protection, we apply a Gaussian blur to adversarial noise with a learnable blur intensity $\sigma > 0$. That is, given an input \mathbf{x} , we start by parameterizing its protection $\hat{\mathbf{x}}$ as follows:

$$\hat{\mathbf{x}} \coloneqq \mathbf{x} + \mathcal{G}(\boldsymbol{\delta}; \sigma), \tag{5}$$

where \mathcal{G} represents the Gaussian blur operation, and δ is a learnable parameter. For image-like inputs, Gaussian blur can be implemented as a depthwise 2D convolution,² where the kernel matrix $H_{\sigma,k} \in \mathbb{R}^{(2k+1)\times(2k+1)}$ is defined by:

$$H_{\sigma,k}(u,v) := G(u) G(v) \text{ for } u,v \in \{-k,\ldots,k\}, \text{ where } G(z) := \frac{1}{\sigma\sqrt{2\pi}} \exp\left(-\frac{z^2}{2\sigma^2}\right).$$
 (6)

The convolution in (6) effectively serves as a low-pass filter; it is equivalent to modulating the Fourier-transformed x by a Gaussian function, given that the Fourier transform of Gaussian kernel is again Gaussian. Here, the blur intensity σ determines the cut-off frequency. We initialize $\omega := \log \sigma$ as learnable parameters instead of directly optimizing σ , primarily to avoid numerical instability.

Power spectrum regularization Given an image x and its protection \hat{x} , we aim to optimize the blur intensity σ of Gaussian blur to minimize their discrepancy in terms of frequency spectrum. To this end, we apply Fast Fourier Transform (FFT) to both x and \hat{x} , and compute RAPSD of them. Specifically, for a 2D Fourier frequency matrix $f \in \mathbb{C}^{hw}$, we first partition the coordinates of f into B bands with respect to the radius from the center; yielding B sets of coordinates $\{\mathcal{B}_b\}_{b=1}^B$. Then, RAPSD is defined by a B-dimensional vector, where the b-th entry is the squared magnitude of the FFT coefficients in \mathcal{B}_b :

$$RAPSD_{b}(\mathbf{f}) := \frac{1}{|\mathcal{B}_{b}|} \sum_{(u,v) \in \mathcal{B}_{b}} |\mathbf{f}(u,v)|^{2}.$$
 (7)

²With this implementation, one can optimize σ using conventional automatic differentiation libraries (*e.g.*, PyTorch), whereas standard implementations often do not support this.

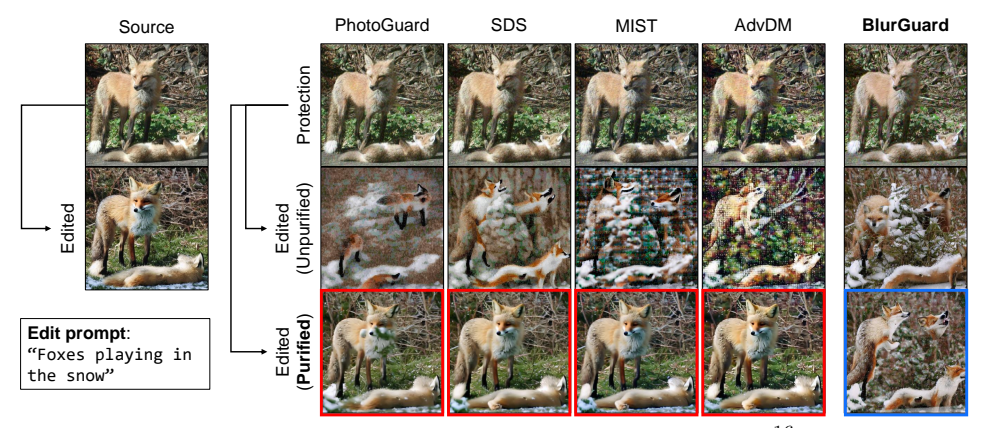


Figure 3: Qualitative comparison of image-to-image generation results ($\epsilon = \frac{16}{255}$). Before purification, all protection methods effectively safeguard the images. However, in the worst-case scenario, the baselines often fail to maintain their protection, producing outputs nearly identical to the original edit. In contrast, BlurGuard continues to generate unrealistic images that do not resemble either the source image or the generation from it. More qualitative results can be found in Figure 12 in Appendix.

Once the frequency matrices f and \hat{f} are obtained from x and \hat{x} , respectively, we define a new *power spectrum regularization* as follows:³

$$L_{\text{freq}}(\hat{\mathbf{x}}, \mathbf{x}) := \left\| \log \frac{\text{RAPSD}(\hat{\mathbf{f}})}{\text{RAPSD}(\mathbf{f})} \right\|_{\infty}$$
 (8)

where $||z||_{\infty} \coloneqq \max_i |z_i|$ is the ℓ_{∞} norm. By minimizing (8), one can ensure that the spectral gaps between \mathbf{x} and $\hat{\mathbf{x}}$ are within a certain margin for all frequencies. BlurGuard uses this regularization primarily to adjust the optimal blur intensity parameter σ .

Per-region adaptation Considering that an image is composed of multiple regions with diverse patterns, it is reasonable to divide the image into several semantic regions and apply different blur intensities; so that the overall frequency characteristics of the perturbed image remain better preserved. To achieve this, we leverage Segment Anything Model (SAM) [40], one of recent image segmentation foundation models, to obtain R binary segmentation masks $\{M_r\}_{r=1}^R$ out of a given image \mathbf{x} . Next, we introduce per-region blur intensity parameters $\{\sigma_r\}_{r=1}^R$, and they are jointly optimized through the following aggregation combined with $\{M_r\}_{r=1}^R$ (\odot is the Hadamard product):

$$\hat{\mathbf{x}} = \mathbf{x} + \sum_{r=1}^{R} M_r \odot \mathcal{G}(\boldsymbol{\delta}; \sigma_r). \tag{9}$$

4.3 Overall Objective

Given an image \mathbf{x} , BlurGuard jointly optimizes the perturbation parameters $\boldsymbol{\delta}$ and blur intensities $\boldsymbol{\sigma} \coloneqq \{\sigma_r\}_{r=1}^R$, and returns the resulting protection $\hat{\mathbf{x}}$ defined as (9). To optimize $\boldsymbol{\delta}$, we combine our proposed power spectrum regularization L_{freq} (8) with an existing adversarial protection objective, say L_{adv} , given a certain adversarial budget; here, we consider an ϵ -ball in ℓ_{∞} distance, following standard practice:

$$\boldsymbol{\delta} = \underset{\|\boldsymbol{\delta}\|_{\infty} \le \epsilon}{\arg\min} \Big(L_{\text{adv}}(\hat{\mathbf{x}}, \mathbf{x}) + \lambda \cdot L_{\text{freq}}(\hat{\mathbf{x}}, \mathbf{x}) \Big), \tag{10}$$

where $\lambda > 0$ is a hyperparameter.⁴ We use iterative optimization (*viz.*, PGD) for solving (10). A slight modification to (2) is that we do not apply $\operatorname{sign}(\cdot)$ for projecting gradients; instead, we simply use ℓ_2 -normalization. This is to reduce gradient noise that can arise from sign-based projection, given that the blurring operation already alters the original gradient direction.

³We average over the channels before applying FFT on \mathbf{x} and $\hat{\mathbf{x}}$, ensuring that their frequency matrices remain two-dimensional.

⁴We fix $\lambda = 10$ throughout all the experiments in this paper.

In terms of σ , on the other hand, we observe that optimizing σ for $L_{\rm adv}$ can be in conflict with $L_{\rm freq}$, causing it to converge to a looser frequency band and thereby affecting robustness. As a simple remedy, we first optimize σ with respect to the power spectrum objective only, *i.e.*, for minimizing $L_{\rm freq}(\hat{\mathbf{x}},\mathbf{x})$, and freeze the learned σ throughout the optimization of δ as in (10). The detailed procedure is provided in Algorithm 1 in the Appendix.

Adversarial objective In principle, our proposed adaptive blurring scheme is versatile and compatible with any form of adversarial objective $L_{\rm adv}$ that aims to protect an image \mathbf{x} from being edited. In our experiments, we adopt the encoder loss $L_{\rm enc}$ of PhotoGuard (1), primarily for simplicity. Here, we take $\mathbf{z}_{\rm target} = \mathbf{0}$, also following Salman et al. [77].

5 Experiments

To verify the effectiveness of BlurGuard, we perform extensive evaluation covering wide AI-powered editing scenarios, including image-to-image generation [73], inpainting-based editing [55], instruction-based editing [7], textual inversion [26], and DreamBooth [74]. We compare various protection methods applicable to editing tasks, considering a fixed ℓ_{∞} -ball of $\epsilon = \frac{16}{255}$ as the adversarial budget following the standard. Our evaluation covers both (a) *naturalness*: how imperceptible the protection is, and (b) *effectiveness*: how much a protected image can deviate from the original image when both are edited. The detailed experimental setups, *e.g.*, datasets, baselines, evaluation metrics, hyperparameters, *etc.*, can be found in Appendix C.

Purification methods To assess the robustness of each protection method, we consider diverse noise purification techniques, including: (a) *JPEG compression*, (b) *JPEG* followed by image upscaling [62], and (c) *Noisy upscaling* [34], which combines Gaussian noise and upscaling for a more aggressive purification. More advanced diffusion-based purification methods are also considered; including (d) Impress [10], (e) DiffPure [63], (f) GrIDPure [102], and (g) PDM-Pure [94]. Details on purification methods can be found in Appendix C.5.

Worst-case effectiveness Unless otherwise noted, we mainly focus on *per-sample worst-case effectiveness* of image protection methods, which compute the "lowest" performance scores after applying all the purification techniques available (*i.e.*, from (a) to (g)) individually for each sample. This comparison assumes an "oracle" attacker equipped with many noise purification techniques, which is essentially closer to more realistic threats.

5.1 Results

Image-to-image generation We test BlurGuard for image-to-image editing based on Stable Diffusion (SD) v1.4 model [73], following previous setups. To effectively evaluate image protection performance across diverse cases, we have curated a new, custom subset of 80 image samples taken from ImageNet [21], coined *ImageNet-Edit*; more details can be found in Appendix C.3.

Table 1 summarizes the results. Overall, we observe that BlurGuard consistently surpasses the baselines tested across all metrics, both in naturalness (up to 30% reduction in LPIPS) and in worst-case robustness (up to 9.8% increase in FID). This observation is further supported qualitatively in Figure 11a. We also remark the high variance of BlurGuard in PSNR naturalness; this is due to that BlurGuard assigns an adaptive amount of perturbation per-image to achieve high naturalness, which is an expected behavior.

In Table 3, we compare the ratio of effectiveness in FID before and after purification. Notably, BlurGuard retains 92.9% of its original protective efficacy even after purification; far surpassing all other methods, which fall between 38.5% and 48.4%. This confirms the superior robustness of BlurGuard to existing purification approaches.

Inpainting Inpainting-based editing incorporates a binary mask information as well as a textual prompt, which can be useful for modifying specific regions (*e.g.*, the surrounding environment or

⁵We report the textual inversion and DreamBooth experiments in Appendix D.1.

⁶We also provide results with SD-v2.1, SD-v3.5, and FLUX.1-dev models in Appendix D.3.

IN-Edit ($\epsilon = \frac{16}{255}$)		Naturalness		Worst-case Effectiveness					
Method	LPIPS ↓	SSIM ↑	PSNR ↑	FID ↑	LPIPS ↑	SSIM↓	PSNR↓	IA ↓	
PhotoGuard [77]	0.34 ± 0.11	0.70 ± 0.11	28.2 ± 0.32	92.21	0.27 ± 0.07	0.73 ± 0.10	29.9 ± 1.07	0.94 ± 0.04	
AdvDM [49]	0.36 ± 0.12	0.74 ± 0.09	28.9 ± 0.28	98.27	0.30 ± 0.08	0.73 ± 0.09	30.2 ± 1.17	0.93 ± 0.04	
Mist [48]	0.35 ± 0.12	0.72 ± 0.10	28.6 ± 0.25	90.96	0.30 ± 0.07	0.71 ± 0.09	29.7 ± 0.86	0.93 ± 0.04	
SDS [96]	$\underline{0.30 \pm 0.09}$	$\underline{0.74 \pm 0.09}$	29.3 ± 0.45	91.48	0.26 ± 0.07	0.73 ± 0.09	30.3 ± 1.23	0.94 ± 0.04	
BlurGuard (Ours)	0.21 ± 0.10	$\boldsymbol{0.93 \pm 0.09}$	31.1 ± 2.29	107.88	0.32 ± 0.09	$\boldsymbol{0.70 \pm 0.09}$	28.8 ± 0.42	$\boldsymbol{0.92 \pm 0.05}$	

(a) Image-to-image generation

Helen $(\epsilon = \frac{16}{255})$		Naturalness		Worst-case Effectiveness					
Method	LPIPS ↓	SSIM ↑	PSNR ↑	FID ↑	LPIPS ↑	SSIM↓	PSNR↓	IA ↓	
PhotoGuard [77]	0.10 ± 0.05	0.91 ± 0.04	35.4 ± 1.71	131.93	0.34 ± 0.08	0.69 ± 0.08	29.5 ± 0.50	0.93 ± 0.04	
AdvDM [49]	$\boldsymbol{0.06 \pm 0.04}$	$\boldsymbol{0.97 \pm 0.02}$	$\textbf{40.4} \pm \textbf{2.29}$	105.26	0.25 ± 0.07	0.76 ± 0.08	30.2 ± 0.70	0.95 ± 0.03	
Mist [48]	0.07 ± 0.04	0.95 ± 0.02	37.3 ± 1.62	109.37	0.27 ± 0.07	0.74 ± 0.07	29.9 ± 0.52	0.95 ± 0.03	
SDS [96]	0.16 ± 0.07	0.92 ± 0.04	35.4 ± 1.75	133.78	0.34 ± 0.08	0.69 ± 0.08	29.6 ± 0.60	0.92 ± 0.03	
DiffusionGuard [18]	0.09 ± 0.05	0.94 ± 0.03	36.6 ± 1.64	123.32	0.32 ± 0.08	0.71 ± 0.08	29.7 ± 0.54	0.93 ± 0.04	
BlurGuard (Ours)	0.11 ± 0.05	$\boldsymbol{0.97 \pm 0.02}$	36.5 ± 2.66	162.92	$\textbf{0.45} \pm \textbf{0.09}$	0.64 ± 0.09	29.0 ± 0.45	$\boldsymbol{0.86 \pm 0.05}$	

(b) Inpainting

MagicBrush ($\epsilon = \frac{16}{255}$)		Naturalness		Worst-case Effectiveness					
Method	LPIPS ↓	SSIM ↑	PSNR ↑	FID ↑	LPIPS ↑	SSIM ↓	PSNR↓	IA ↓	
PhotoGuard [77]	0.19 ± 0.10	0.74 ± 0.09	31.1 ± 0.22	96.23	0.21 ± 0.09	0.73 ± 0.11	30.7 ± 1.50	0.96 ± 0.03	
AdvDM [49]	0.27 ± 0.08	0.76 ± 0.07	28.9 ± 0.24	123.39	0.30 ± 0.09	0.67 ± 0.13	30.2 ± 1.25	0.93 ± 0.04	
Mist [48]	0.26 ± 0.09	0.74 ± 0.08	28.6 ± 0.17	123.54	0.30 ± 0.09	0.66 ± 0.12	29.8 ± 0.94	0.93 ± 0.04	
SDS [96]	0.23 ± 0.07	0.74 ± 0.07	29.1 ± 0.37	115.23	0.27 ± 0.09	0.68 ± 0.13	30.3 ± 1.38	0.94 ± 0.04	
EditShield [15]	0.36 ± 0.13	0.75 ± 0.09	$\underline{31.0\pm0.23}$	120.13	$\underline{0.33 \pm 0.09}$	$\underline{0.65 \pm 0.13}$	29.9 ± 1.26	$\underline{0.93 \pm 0.04}$	
BlurGuard (Ours)	0.20 ± 0.08	$\boldsymbol{0.89 \pm 0.07}$	30.1 ± 1.76	138.22	$\boldsymbol{0.36 \pm 0.10}$	$\textbf{0.64} \pm \textbf{0.12}$	28.8 ± 0.55	$\boldsymbol{0.90 \pm 0.06}$	

(c) Instruction-based editing

Table 1: Comparisons of image protection within ℓ_{∞} -balls of $\epsilon = \frac{16}{255}$. Naturalness indicates how much a protected image deviates from the original. Worst-case effectiveness is measured after applying all purification methods to the protected image. The best is highlighted in **bold**, while the second-best in underlined.

IGBench ($\varepsilon = \frac{16}{255}$)	Natur	alness	Worst-ca	se Effect. (Seen)	Worst-case Effect. (Unseen)		
Method	LPIPS ↓	SSIM ↑	FID ↑	PSNR↓	FID ↑	PSNR↓	
PhotoGuard [77]	0.03 ± 0.02	0.96 ± 0.02	103.83	37.2 ± 14.2	67.05	35.5 ± 8.2	
AdvDM [49]	$\overline{0.03 \pm 0.02}$	0.97 ± 0.02	125.66	35.3 ± 10.3	71.06	35.4 ± 7.0	
Mist [48]	$\overline{0.02\pm0.01}$	0.98 ± 0.01	112.23	37.1 ± 14.2	58.48	36.4 ± 9.8	
SDS [96]	0.05 ± 0.03	$\overline{0.96 \pm 0.02}$	113.30	37.1 ± 14.2	83.91	35.6 ± 7.2	
DiffusionGuard [18]	$\underline{0.03 \pm 0.02}$	0.97 ± 0.02	134.25	37.1 ± 14.2	61.32	35.9 ± 9.9	
BlurGuard (Ours)	0.03 ± 0.02	$\boldsymbol{0.99 \pm 0.01}$	140.82	34.9 ± 17.0	90.32	$\textbf{35.3} \pm \textbf{8.9}$	

Table 2: Comparison of image protection for inpainting under mask variability. We test our method on InpaintGuardBench (IGBench) [18] that provides unseen shapes of mask not exposed during each protection phase. The best is highlighted in **bold**, while the second-best in underlined.

objects) while preserving others (*e.g.*, a person's face) Consequently, image protections should be confined to the facial region rather than applied to the entire image, and we follow this setup. For evaluation, we use the Helen dataset [44], following Cao et al. [10].

As reported in Table 1, BlurGuard again achieves the strongest worst-case effectiveness, while maintaining high naturalness; for example, under the same $\epsilon = \frac{16}{255}$ budget, BlurGuard finds perturbations that achieve 0.45 LPIPS on average in terms of worst-case effectiveness, which is 32.3% higher than the second-best baseline. Qualitative results can be found in Appendix E.

To further evaluate the effectiveness of BlurGuard in realistic inpainting scenarios with diverse editing masks, we assess its robustness under mask variability using the InpaintGuardBench [18]. Each image is tested with six masks, including both "seen" (used for protection) and "unseen" (novel) ones.

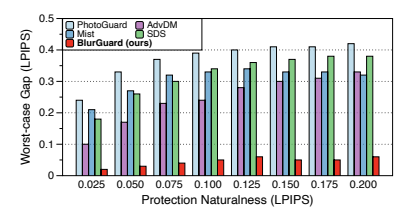


Figure 4: Comparison of protection naturalness vs. worst-case effectiveness (both in LPIPS) across different protection methods.

$(\epsilon = \frac{16}{255})$	Puri	fied?	Robustness
Method	X (A)	√ (B)	(B/A; %)
PhotoGuard	202.0	92.2	45.6
AdvDM	255.6	98.3	38.5
Mist	233.7	91.0	38.9
SDS	189.0	91.5	48.4
BlurGuard	116.2	107.9	92.9

Table 3: Comparison of pro- Table 4: Results of black-box

Method	FID ↑	$\textbf{LPIPS} \uparrow$	SSIM↓
PhotoGuard	134.0	0.36	0.66
AdvDM	150.8	0.40	0.69
Mist	147.2	0.40	0.68
SDS	142.6	0.36	0.68
BlurGuard	153.1	0.41	0.62

tection effectiveness in FID image-to-image on ImageNetbefore and after purification on ImageNet-Edit. Best result is marked in **bold**. Edit (SD-v1.4 \rightarrow SD-v2.1). We use $\epsilon = \frac{16}{255}$ in ℓ_{∞} . Best result is marked in **bold**.

IN-Edit ($\varepsilon = \frac{16}{255}$)		Naturalness		Worst-case Effectiveness					
Method	LPIPS ↓	SSIM ↑	PSNR ↑	FID ↑	LPIPS ↑	SSIM↓	PSNR↓	IA↓	
AdvDM [49]	0.36 ± 0.12	0.74 ± 0.09	28.9 ± 0.28	98.27	0.30 ± 0.08	0.73 ± 0.09	30.2 ± 1.17	$0.93 \pm 0.04 \\ 0.93 \pm 0.05$	
+ BlurGuard	0.25 ± 0.07	0.81 ± 0.09	30.1 ± 2.19	101.84	0.35 ± 0.09	0.70 ± 0.09	28.2 \pm 2.03		
Mist [48]	0.35 ± 0.12	0.72 ± 0.10	28.6 ± 0.25	90.96	0.30 ± 0.07	0.71 ± 0.09	29.7 ± 0.86	0.93 ± 0.04	
+ BlurGuard	0.33 ± 0.11	0.86 ± 0.08	32.3 ± 2.21	137.91	0.42 ± 0.10	0.63 ± 0.07	$\mathbf{28.8 \pm 0.47}$	0.89 ± 0.06	

Table 5: BlurGuard combined with other adversarial objectives, viz., AdvDM and Mist, on ImageNet-Edit. We consider ℓ_{∞} protections within $\epsilon = \frac{16}{255}$.

As shown in Table 2, BlurGuard consistently maintains strong protection across these variations, demonstrating robustness to practical editing conditions.

Instruction-based editing We also evaluate BlurGuard on instruction-based editing scenarios, focusing on InstructPix2Pix [7]; a fine-tuned diffusion model specifically to follow natural-language editing instructions. We use MagicBrush [98] dataset for the evaluation. As shown in Table 1c, BlurGuard shows superior worst-case protection effectiveness across all proposed metrics, while maintaining high imperceptibility competitive to the best baseline.

Naturalness vs. robustness Figure 4 compares how the worst-case gap (measured by LPIPS) varies with the naturalness of each protection method (also measured by LPIPS) on image-to-image generation. Here, we define the worst-case gap as the degradation in protection effectiveness under the strongest purification method. To this end, we construct a histogram of pairs of these two LPIPS values for each method, drawing samples by varying the adversarial budget ϵ from $\frac{1}{255}$ to $\frac{16}{255}$. The results reveal that, unlike other methods that suffer from significant performance degradation after purification, BlurGuard consistently maintains a nearly zero performance gap across all LPIPS levels.

Black-box transfer We further evaluate BlurGuard on black-box transfer. Specifically, we test image protections optimized from SD-v1.4 to other models; here we consider SD-v2.1. Results in Table 4 show that BlurGuard maintains its effectiveness in black-box setup as well, suggesting that adversarial noise in controlled frequency regime generalizes more effectively across models. Qualitative results can be found in Figure 13 in Appendix. We also test SD-v3.5, FLUX.1-dev [43], and a GAN-based SimSwap [14] as additional target models, as reported in Appendix D.2.

BlurGuard with other adversarial objectives To demonstrate that BlurGuard operates in a simple plug-and-play manner, we test its compatibility with other adversarial objectives: AdvDM [49], which directly maximizes the denoising loss, and Mist [48], which jointly attacks the encoder and denoiser. As shown in Table 5, BlurGuard consistently enhances both naturalness and worst-case effectiveness across these objectives, demonstrating its broad applicability to diverse protection frameworks.

5.2 Ablation study

We perform an ablation study to validate the effectiveness of the individual components in BlurGuard. Throughout this study, we consider image-to-image generation tasks using SD-v1.4 with $\epsilon = \frac{16}{255}$. Additional ablation studies can be found in Appendix D.4.

	Natur	alness	Worst-case Effect.		
	SSIM ↑	PSNR ↑	LPIPS ↑	FID ↑	
BlurGuard	0.93 ± 0.09	31.1 ± 2.29	0.32 ± 0.09	107.88	
w/o Adaptive blurring					
$\sigma = 0.0$ (const.)	0.55 ± 0.14	32.9 ± 2.49	0.19 ± 0.07	65.94	
$\sigma = 0.5$ (const.)	0.59 ± 0.13	31.9 ± 1.92	0.22 ± 0.10	79.66	
$\sigma = 1.0$ (const.)	0.77 ± 0.17	31.6 ± 1.44	0.31 ± 0.14	94.00	
w/o Per-region masks	0.94 ± 0.09	31.1 ± 2.51	0.29 ± 0.09	96.57	
w/o Spectrum reg. $(\lambda = 0.0)$					
learned σ	0.69 ± 0.12	31.1 ± 1.69	0.40 ± 0.11	113.97	
learned σ , $\epsilon = \frac{4}{255}$	0.91 ± 0.06	32.0 ± 1.13	0.19 ± 0.04	28.57	
$\sigma = 0.0$	0.70 ± 0.11	28.2 ± 0.32	0.27 ± 0.07	92.21	

Table 6: Ablation study on BlurGuard. By default, we consider the ℓ_{∞} constraint within $\epsilon = \frac{16}{255}$.

Method	Inference Time (s)
PhotoGuard	8.836 ± 0.005
Mist	31.267 ± 0.044
AdvDM	31.103 ± 0.008
SDS	12.493 ± 0.016
BlurGuard	31.071 ± 0.012
- Semantic masking	3.019 ± 0.001
 Adaptive blurring 	5.367 ± 0.002
 PGD updates 	22.685 ± 0.010

Table 7: Comparison of inference time (in seconds) measured on a single NVIDIA A100 (80GB) instance.

Adaptive blurring To validate the effectiveness of our learnable Gaussian blur scheme, we compare BlurGuard with ablations where the blur intensity σ are all fixed as constant throughout optimizing δ . Specifically, we test $\sigma=0,\,0.5,\,$ and $1.0.\,$ The results in Table 6 ("w/o Adaptive blurring") confirm that our adaptive σ provides more effective protection by better aligning the frequency bands of the perturbation with the image. The significantly low SSIMs observed from the fixed- σ configurations, despite their high PSNR scores, indicate that constant blurring often degrade image likelihood even when the perturbation magnitude is low. For example, fixed blurring may fail to account for textural characteristics of given image, leading to both unnatural and weak protection.

Semantic-aware masks Next, we evaluate how our per-region blurring mechanism enhances BlurGuard, compared to its ablation ("w/o Per-region masks") that learns a single σ for the entire image. Table 6 shows that the per-region approach provides higher protection effectiveness in worst-case scenarios, while being competitive in naturalness. This indicates that robust protection benefits from varying blurring intensities for different image regions depending on their frequency spectrum.

Power spectrum regularization We test two ablations for our proposed power spectrum regularization: (a) $\lambda=0$ while learning σ during the first training stage, and (b) those even without σ , which is essentially equivalent to PhotoGuard (1) in this experiment. Overall, we observe that spectrum regularization plays a crucial role in preserving naturalness; although the adaptive blurring scheme already enhances worst-case effectiveness, it compromises naturalness without the regularization as the adversarial objective $L_{\rm adv}$ in (10) alters the frequency spectrum. For example, the "learned σ , $\epsilon=\frac{4}{255}$ " ablation yields far weaker worst-case effectiveness than BlurGuard while it maintains similar imperceptibility metrics. These results demonstrate that the spectrum regularization we propose induces a more effective protection without sacrificing visual imperceptibility.

Computational overhead We report the computational overhead caused by each component of BlurGuard by measuring per-sample inference time (on a single NVIDIA A100 80GB GPU instance) as shown in Table 7. Overall, we observe that BlurGuard introduces overhead no greater than existing methods such as Mist and AdvDM, with the proposed adaptive blurring and semantic-aware masking pipeline accounting for only a small portion of the total time.

6 Conclusion

We introduce BlurGuard, a simple-yet-effective framework designed to protect images from unauthorized editing via generative models. BlurGuard tackles the current challenge of protection methods against purification by crafting adversarial noise that remains closer to in-distribution. We conduct extensive experiments to validate the effectiveness of BlurGuard, even introducing an "oracle" attacker equipped with the strongest purification among diverse options. The results consistently show that BlurGuard enhances robustness against existing purification methods, highlighting the potential of adversarial examples with naturalness as a promising direction for future research.

Acknowledgements

This work was supported by the Institute of Information & Communications Technology Planning & Evaluation (IITP) grants funded by the Korea government (MSIT) (No. RS-2019-II190079, Artificial Intelligence Graduate School Program (Korea University); No. IITP-2025-RS-2025-02304828, Artificial Intelligence Star Fellowship Support Program to Nurture the Best Talents; No. IITP-2025-RS-2024-00436857, Information Technology Research Center (ITRC)), the National Research Foundation of Korea (NRF) grant funded by the Korea government (MSIT) (No. RS-2025-23523603), and the Korea Creative Content Agency grant funded by the Ministry of Culture, Sports and Tourism (No. RS-2025-00345025).

References

- Namhyuk Ahn, Wonhyuk Ahn, KiYoon Yoo, Daesik Kim, and Seung-Hun Nam. Imperceptible protection against style imitation from diffusion models. arXiv preprint arXiv:2403.19254, 2024.
- [2] Namhyuk Ahn, KiYoon Yoo, Wonhyuk Ahn, Daesik Kim, and Seung-Hun Nam. Nearly zero-cost protection against mimicry by personalized diffusion models. In *Proceedings of the IEEE/CVF Conference on Computer Vision and Pattern Recognition*, 2025. URL https://arxiv.org/abs/2412.11423.
- [3] Anish Athalye, Nicholas Carlini, and David Wagner. Obfuscated gradients give a false sense of security: Circumventing defenses to adversarial examples. In Jennifer Dy and Andreas Krause, editors, *Proceedings of the 35th International Conference on Machine Learning*, volume 80 of *Proceedings of Machine Learning Research*, pages 274–283. PMLR, 10–15 Jul 2018. URL https://proceedings.mlr.press/v80/athalye18a.html.
- [4] James Betker, Gabriel Goh, Li Jing, Tim Brooks, Jianfeng Wang, Linjie Li, Long Ouyang, Juntang Zhuang, Joyce Lee, Yufei Guo, et al. Improving image generation with better captions, 2023. URL https://cdn.openai.com/papers/dall-e-3.pdf.
- [5] Battista Biggio, Igino Corona, Davide Maiorca, Blaine Nelson, Nedim Šrndić, Pavel Laskov, Giorgio Giacinto, and Fabio Roli. Evasion attacks against machine learning at test time. In Machine Learning and Knowledge Discovery in Databases: European Conference, ECML PKDD 2013, Prague, Czech Republic, September 23-27, 2013, Proceedings, Part III 13, pages 387–402. Springer, 2013.
- [6] Nicolo Bonettini, Edoardo Daniele Cannas, Sara Mandelli, Luca Bondi, Paolo Bestagini, and Stefano Tubaro. Video face manipulation detection through ensemble of CNNs. In 25th International Conference on Pattern Recognition, pages 5012–5019. IEEE, 2020.
- [7] Tim Brooks, Aleksander Holynski, and Alexei A Efros. InstructPix2Pix: Learning to follow image editing instructions. In *Proceedings of the IEEE/CVF Conference on Computer Vision* and Pattern Recognition, pages 18392–18402, 2023.
- [8] Tim Brooks, Bill Peebles, Connor Holmes, Will DePue, Yufei Guo, Li Jing, David Schnurr, Joe Taylor, Troy Luhman, Eric Luhman, Clarence Ng, Ricky Wang, and Aditya Ramesh. Video generation models as world simulators. *OpenAI Blog*, 2024.
- [9] Geoffrey J Burton and Ian R Moorhead. Color and spatial structure in natural scenes. Applied Optics, 26(1):157–170, 1987.
- [10] Bochuan Cao, Changjiang Li, Ting Wang, Jinyuan Jia, Bo Li, and Jinghui Chen. Impress: Evaluating the resilience of imperceptible perturbations against unauthorized data usage in diffusion-based generative AI. *Advances in Neural Information Processing Systems*, 36: 10657–10677, 2023.
- [11] Qiong Cao, Li Shen, Weidi Xie, Omkar M. Parkhi, and Andrew Zisserman. Vggface2: A dataset for recognising faces across pose and age. In *Proceedings of the IEEE Conference on Automatic Face and Gesture Recognition*, 2018. URL https://arxiv.org/abs/1710.08092.

- [12] Nicholas Carlini and David Wagner. Towards evaluating the robustness of neural networks. In *IEEE Symposium on Security and Privacy*, pages 39–57. IEEE, 2017.
- [13] Jianqi Chen, Hao Chen, Keyan Chen, Yilan Zhang, Zhengxia Zou, and Zhenwei Shi. Diffusion models for imperceptible and transferable adversarial attack. *IEEE Transactions on Pattern Analysis and Machine Intelligence*, 47(2):961–977, 2025. doi: 10.1109/TPAMI.2024.3480519.
- [14] Renwang Chen, Xuanhong Chen, Bingbing Ni, and Yanhao Ge. Simswap: An efficient framework for high fidelity face swapping. In *Proceedings of the 28th ACM international conference on multimedia*, pages 2003–2011, 2020.
- [15] Ruoxi Chen, Haibo Jin, Yixin Liu, Jinyin Chen, Haohan Wang, and Lichao Sun. Editshield: Protecting unauthorized image editing by instruction-guided diffusion models. In *European Conference on Computer Vision*, pages 126–142. Springer, 2024.
- [16] Zilong Chen, Feng Wang, Yikai Wang, and Huaping Liu. Text-to-3d using gaussian splatting. In Proceedings of the IEEE/CVF Conference on Computer Vision and Pattern Recognition, pages 21401–21412, 2024.
- [17] Valeriia Cherepanova, Micah Goldblum, Harrison Foley, Shiyuan Duan, John P Dickerson, Gavin Taylor, and Tom Goldstein. LowKey: Leveraging adversarial attacks to protect social media users from facial recognition. In *International Conference on Learning Representations*, 2021. URL https://openreview.net/forum?id=hJmtwocEqzc.
- [18] June Suk Choi, Kyungmin Lee, Jongheon Jeong, Saining Xie, Jinwoo Shin, and Kimin Lee. DiffusionGuard: A robust defense against malicious diffusion-based image editing. *arXiv* preprint arXiv:2410.05694, 2024.
- [19] Yujin Choi, Jinseong Park, Hoki Kim, Jaewook Lee, and Saerom Park. Fair sampling in diffusion models through switching mechanism. In *Proceedings of the AAAI Conference on Artificial Intelligence*, volume 38, pages 21995–22003, 2024.
- [20] Yingqian Cui, Jie Ren, Han Xu, Pengfei He, Hui Liu, Lichao Sun, Yue Xing, and Jiliang Tang. DiffusionShield: A watermark for copyright protection against generative diffusion models. *arXiv preprint arXiv:2306.04642*, 2023.
- [21] Jia Deng, Wei Dong, Richard Socher, Li-Jia Li, Kai Li, and Li Fei-Fei. ImageNet: A large-scale hierarchical image database. In *2009 IEEE Conference on Computer Vision and Pattern Recognition*, pages 248–255, 2009. doi: 10.1109/CVPR.2009.5206848.
- [22] Prafulla Dhariwal and Alexander Nichol. Diffusion models beat gans on image synthesis. *Advances in Neural Information Processing Systems*, 34:8780–8794, 2021.
- [23] Patrick Esser, Sumith Kulal, Andreas Blattmann, Rahim Entezari, Jonas Müller, Harry Saini, Yam Levi, Dominik Lorenz, Axel Sauer, Frederic Boesel, et al. Scaling rectified flow transformers for high-resolution image synthesis. In *Forty-first International Conference on Machine Learning*, 2024.
- [24] Pierre Fernandez, Guillaume Couairon, Hervé Jégou, Matthijs Douze, and Teddy Furon. The stable signature: Rooting watermarks in latent diffusion models. In *Proceedings of the IEEE/CVF International Conference on Computer Vision*, pages 22466–22477, 2023.
- [25] Felix Friedrich, Manuel Brack, Lukas Struppek, Dominik Hintersdorf, Patrick Schramowski, Sasha Luccioni, and Kristian Kersting. Fair diffusion: Instructing text-to-image generation models on fairness. *arXiv preprint arXiv:2302.10893*, 2023.
- [26] Rinon Gal, Yuval Alaluf, Yuval Atzmon, Or Patashnik, Amit Haim Bermano, Gal Chechik, and Daniel Cohen-or. An image is worth one word: Personalizing text-to-image generation using textual inversion. In *The Eleventh International Conference on Learning Representations*, 2023. URL https://openreview.net/forum?id=NAQvF08TcyG.
- [27] Rohit Gandikota, Joanna Materzynska, Jaden Fiotto-Kaufman, and David Bau. Erasing concepts from diffusion models. In *Proceedings of the IEEE/CVF International Conference on Computer Vision*, pages 2426–2436, 2023.

- [28] Rohit Gandikota, Hadas Orgad, Yonatan Belinkov, Joanna Materzyńska, and David Bau. Unified concept editing in diffusion models. In *Proceedings of the IEEE/CVF Winter Conference on Applications of Computer Vision*, pages 5111–5120, 2024.
- [29] Ian J. Goodfellow, Jonathon Shlens, and Christian Szegedy. Explaining and harnessing adversarial examples, 2015. URL https://arxiv.org/abs/1412.6572.
- [30] Chuan Guo, Mayank Rana, Moustapha Cisse, and Laurens van der Maaten. Countering adversarial images using input transformations. In *International Conference on Learning Representations*, 2018. URL https://openreview.net/forum?id=SyJ7ClWCb.
- [31] Chuan Guo, Jared S. Frank, and Kilian Q. Weinberger. Low frequency adversarial perturbation, 2019. URL https://arxiv.org/abs/1809.08758.
- [32] Alvin Heng and Harold Soh. Selective amnesia: A continual learning approach to forgetting in deep generative models. *Advances in Neural Information Processing Systems*, 36, 2024.
- [33] Jonathan Ho, Ajay Jain, and Pieter Abbeel. Denoising diffusion probabilistic models. *Advances in Neural Information Processing Systems*, 33:6840–6851, 2020.
- [34] Robert Hönig, Javier Rando, Nicholas Carlini, and Florian Tramèr. Adversarial perturbations cannot reliably protect artists from generative AI. *ICML GenAI and Law workshop*, 2024.
- [35] Runyi Hu, Jie Zhang, Ting Xu, Jiwei Li, and Tianwei Zhang. Robust-wide: Robust watermarking against instruction-driven image editing. In *European Conference on Computer Vision*, pages 20–37. Springer, 2025.
- [36] Guillaume Jeanneret, Loïc Simon, and Frédéric Jurie. Adversarial counterfactual visual explanations. In *Proceedings of the IEEE/CVF Conference on Computer Vision and Pattern Recognition*, pages 16425–16435, 2023.
- [37] Minguk Kang, Jun-Yan Zhu, Richard Zhang, Jaesik Park, Eli Shechtman, Sylvain Paris, and Taesung Park. Scaling up GANs for text-to-image synthesis. In *Proceedings of the IEEE/CVF Conference on Computer Vision and Pattern Recognition*, pages 10124–10134, 2023.
- [38] Tero Karras, Miika Aittala, Timo Aila, and Samuli Laine. Elucidating the design space of diffusion-based generative models. *Advances in Neural Information Processing Systems*, 35: 26565–26577, 2022.
- [39] Jaehyung Kim, Jongheon Jeong, and Jinwoo Shin. M2m: Imbalanced classification via majorto-minor translation. In *Proceedings of the IEEE/CVF conference on computer vision and pattern recognition*, pages 13896–13905, 2020.
- [40] Alexander Kirillov, Eric Mintun, Nikhila Ravi, Hanzi Mao, Chloe Rolland, Laura Gustafson, Tete Xiao, Spencer Whitehead, Alexander C Berg, Wan-Yen Lo, et al. Segment anything. In *Proceedings of the IEEE/CVF International Conference on Computer Vision*, pages 4015–4026, 2023.
- [41] Pavel Korshunov and Sébastien Marcel. Deepfakes: A new threat to face recognition? assessment and detection. *arXiv preprint arXiv:1812.08685*, 2018.
- [42] Nupur Kumari, Bingliang Zhang, Sheng-Yu Wang, Eli Shechtman, Richard Zhang, and Jun-Yan Zhu. Ablating concepts in text-to-image diffusion models. In *Proceedings of the IEEE/CVF International Conference on Computer Vision*, pages 22691–22702, 2023.
- [43] Black Forest Labs, Stephen Batifol, Andreas Blattmann, Frederic Boesel, Saksham Consul, Cyril Diagne, Tim Dockhorn, Jack English, Zion English, Patrick Esser, Sumith Kulal, Kyle Lacey, Yam Levi, Cheng Li, Dominik Lorenz, Jonas Müller, Dustin Podell, Robin Rombach, Harry Saini, Axel Sauer, and Luke Smith. Flux.1 kontext: Flow matching for in-context image generation and editing in latent space, 2025. URL https://arxiv.org/abs/2506.15742.
- [44] Vuong Le, Jonathan Brandt, Zhe Lin, Lubomir Bourdev, and Thomas S Huang. Interactive facial feature localization. In *Computer Vision–ECCV 2012: 12th European Conference on Computer Vision, Florence, Italy, October 7-13, 2012, Proceedings, Part III 12*, pages 679–692. Springer, 2012.

- [45] Minjong Lee and Dongwoo Kim. Robust evaluation of diffusion-based adversarial purification. In Proceedings of the IEEE/CVF International Conference on Computer Vision, pages 134–144, 2023.
- [46] Junnan Li, Dongxu Li, Silvio Savarese, and Steven Hoi. BLIP-2: Bootstrapping languageimage pre-training with frozen image encoders and large language models. In *International Conference on Machine Learning*, pages 19730–19742. PMLR, 2023.
- [47] Yuezun Li, Xin Yang, Pu Sun, Honggang Qi, and Siwei Lyu. Celeb-df: A large-scale challenging dataset for deepfake forensics. In *Proceedings of the IEEE/CVF Conference on Computer Vision and Pattern Recognition*, pages 3207–3216, 2020.
- [48] Chumeng Liang and Xiaoyu Wu. Mist: Towards improved adversarial examples for diffusion models. *arXiv preprint arXiv:2305.12683*, 2023.
- [49] Chumeng Liang, Xiaoyu Wu, Yang Hua, Jiaru Zhang, Yiming Xue, Tao Song, Zhengui Xue, Ruhui Ma, and Haibing Guan. Adversarial example does good: Preventing painting imitation from diffusion models via adversarial examples. In *International Conference on Machine Learning*, pages 20763–20786. PMLR, 2023.
- [50] Li Lin, Xinan He, Yan Ju, Xin Wang, Feng Ding, and Shu Hu. Preserving fairness generalization in deepfake detection. In *Proceedings of the IEEE/CVF Conference on Computer Vision and Pattern Recognition*, pages 16815–16825, 2024.
- [51] Hanwen Liu, Zhicheng Sun, and Yadong Mu. Countering personalized text-to-image generation with influence watermarks. In *Proceedings of the IEEE/CVF Conference on Computer Vision and Pattern Recognition*, pages 12257–12267, 2024.
- [52] Ruoshi Liu, Rundi Wu, Basile Van Hoorick, Pavel Tokmakov, Sergey Zakharov, and Carl Vondrick. Zero-1-to-3: Zero-shot one image to 3d object. In *Proceedings of the IEEE/CVF International Conference on Computer Vision*, pages 9298–9309, 2023.
- [53] Cheng Lu, Yuhao Zhou, Fan Bao, Jianfei Chen, Chongxuan Li, and Jun Zhu. DPM-Solver++: Fast solver for guided sampling of diffusion probabilistic models. *arXiv* preprint *arXiv*:2211.01095, 2022.
- [54] Shilin Lu, Zihan Zhou, Jiayou Lu, Yuanzhi Zhu, and Adams Wai-Kin Kong. Robust water-marking using generative priors against image editing: From benchmarking to advances. *arXiv* preprint arXiv:2410.18775, 2024.
- [55] Andreas Lugmayr, Martin Danelljan, Andres Romero, Fisher Yu, Radu Timofte, and Luc Van Gool. Repaint: Inpainting using denoising diffusion probabilistic models. In *Proceedings* of the IEEE/CVF Conference on Computer Vision and Pattern Recognition, pages 11461– 11471, 2022.
- [56] Cheng Luo, Qinliang Lin, Weicheng Xie, Bizhu Wu, Jinheng Xie, and Linlin Shen. Frequency-driven imperceptible adversarial attack on semantic similarity. In *Proceedings of the IEEE/CVF Conference on Computer Vision and Pattern Recognition*, pages 15315–15324, 2022.
- [57] Aleksander Madry, Aleksandar Makelov, Ludwig Schmidt, Dimitris Tsipras, and Adrian Vladu. Towards deep learning models resistant to adversarial attacks. In *International Conference on Learning Representations*, 2018. URL https://openreview.net/forum?id=rJzIBfZAb.
- [58] Chenlin Meng, Yutong He, Yang Song, Jiaming Song, Jiajun Wu, Jun-Yan Zhu, and Stefano Ermon. SDEdit: Guided image synthesis and editing with stochastic differential equations. In *International Conference on Learning Representations*, 2022.
- [59] Xiaoyue Mi, Fan Tang, Juan Cao, Peng Li, and Yang Liu. Visual-friendly concept protection via selective adversarial perturbations. *CoRR*, abs/2408.08518, 2024. URL https://doi.org/10.48550/arXiv.2408.08518.
- [60] Rui Min, Sen Li, Hongyang Chen, and Minhao Cheng. A watermark-conditioned diffusion model for IP protection. In *European Conference on Computer Vision*, pages 104–120. Springer, 2024.

- [61] Yisroel Mirsky and Wenke Lee. The creation and detection of deepfakes: A survey. *ACM Computing Surveys (CSUR)*, 54(1):1–41, 2021.
- [62] Aamir Mustafa, Salman H. Khan, Munawar Hayat, Jianbing Shen, and Ling Shao. Image superresolution as a defense against adversarial attacks. *IEEE Transactions on Image Processing*, 29:1711–1724, 2020. ISSN 1941-0042. doi: 10.1109/tip.2019.2940533. URL http://dx.doi.org/10.1109/TIP.2019.2940533.
- [63] Weili Nie, Brandon Guo, Yujia Huang, Chaowei Xiao, Arash Vahdat, and Animashree Anandkumar. Diffusion models for adversarial purification. In Kamalika Chaudhuri, Stefanie Jegelka, Le Song, Csaba Szepesvari, Gang Niu, and Sivan Sabato, editors, *Proceedings of the 39th International Conference on Machine Learning*, volume 162 of *Proceedings of Machine Learning Research*, pages 16805–16827. PMLR, 17–23 Jul 2022. URL https://proceedings.mlr.press/v162/nie22a.html.
- [64] Takuto Onikubo and Yusuke Matsui. High-Frequency Anti-Dreambooth: Robust defense against personalized image synthesis. In *ECCV 2024 Workshop The Dark Side of Generative Als and Beyond*, 2024.
- [65] OpenAI. GPT-40 system card, 2024. URL https://arxiv.org/abs/2410.21276.
- [66] Sen Peng, Mingyue Wang, Jianfei He, Jijia Yang, and Xiaohua Jia. Cat: Contrastive adversarial training for evaluating the robustness of protective perturbations in latent diffusion models. *arXiv preprint arXiv:2502.07225*, 2025.
- [67] Dustin Podell, Zion English, Kyle Lacey, Andreas Blattmann, Tim Dockhorn, Jonas Müller, Joe Penna, and Robin Rombach. SDXL: Improving latent diffusion models for high-resolution image synthesis. In *The Twelfth International Conference on Learning Representations*, 2024. URL https://openreview.net/forum?id=di52zR8xgf.
- [68] Andrea Polesel, Giovanni Ramponi, and V John Mathews. Image enhancement via adaptive unsharp masking. *IEEE transactions on image processing*, 9(3):505–510, 2000.
- [69] Adam Polyak, Amit Zohar, Andrew Brown, Andros Tjandra, Animesh Sinha, Ann Lee, Apoorv Vyas, Bowen Shi, Chih-Yao Ma, Ching-Yao Chuang, et al. Movie Gen: A cast of media foundation models. *arXiv preprint arXiv:2410.13720*, 2024.
- [70] Ben Poole, Ajay Jain, Jonathan T. Barron, and Ben Mildenhall. Dreamfusion: Text-to-3d using 2d diffusion. In *The Eleventh International Conference on Learning Representations*, 2023. URL https://openreview.net/forum?id=FjNys5c7VyY.
- [71] Alec Radford, Jong Wook Kim, Chris Hallacy, Aditya Ramesh, Gabriel Goh, Sandhini Agarwal, Girish Sastry, Amanda Askell, Pamela Mishkin, Jack Clark, et al. Learning transferable visual models from natural language supervision. In *International Conference on Machine Learning*, pages 8748–8763. PMLR, 2021.
- [72] Severi Rissanen, Markus Heinonen, and Arno Solin. Generative modelling with inverse heat dissipation. In *The Eleventh International Conference on Learning Representations*, 2023. URL https://openreview.net/forum?id=4PJUBT9f201.
- [73] Robin Rombach, Andreas Blattmann, Dominik Lorenz, Patrick Esser, and Björn Ommer. High-resolution image synthesis with latent diffusion models. In *Proceedings of the IEEE/CVF Conference on Computer Vision and Pattern Recognition*, pages 10684–10695, 2022.
- [74] Nataniel Ruiz, Yuanzhen Li, Varun Jampani, Yael Pritch, Michael Rubinstein, and Kfir Aberman. Dreambooth: Fine tuning text-to-image diffusion models for subject-driven generation. In *Proceedings of the IEEE/CVF Conference on Computer Vision and Pattern Recognition*, pages 22500–22510, 2023.
- [75] Chitwan Saharia, William Chan, Saurabh Saxena, Lala Li, Jay Whang, Emily L Denton, Kamyar Ghasemipour, Raphael Gontijo Lopes, Burcu Karagol Ayan, Tim Salimans, et al. Photorealistic text-to-image diffusion models with deep language understanding. *Advances in Neural Information Processing Systems*, 35:36479–36494, 2022.

- [76] Chitwan Saharia, Jonathan Ho, William Chan, Tim Salimans, David J Fleet, and Mohammad Norouzi. Image super-resolution via iterative refinement. *IEEE Transactions on Pattern Analysis and Machine Intelligence*, 45(4):4713–4726, 2022.
- [77] Hadi Salman, Alaa Khaddaj, Guillaume Leclerc, Andrew Ilyas, and Aleksander Madry. Raising the cost of malicious AI-powered image editing. In *Proceedings of the 40th International Conference on Machine Learning*, 2023.
- [78] Pouya Samangouei, Maya Kabkab, and Rama Chellappa. Defense-GAN: Protecting classifiers against adversarial attacks using generative models. In *International Conference on Learning Representations*, 2018. URL https://openreview.net/forum?id=BkJ3ibb0-.
- [79] Shawn Shan, Emily Wenger, Jiayun Zhang, Huiying Li, Haitao Zheng, and Ben Y Zhao. Fawkes: Protecting privacy against unauthorized deep learning models. In *29th USENIX Security Symposium*, pages 1589–1604, 2020.
- [80] Shawn Shan, Jenna Cryan, Emily Wenger, Haitao Zheng, Rana Hanocka, and Ben Y Zhao. Glaze: Protecting artists from style mimicry by text-to-image models. In *32nd USENIX Security Symposium*, pages 2187–2204, 2023.
- [81] Yash Sharma, Gavin Weiguang Ding, and Marcus A. Brubaker. On the effectiveness of low frequency perturbations. In *Proceedings of the 28th International Joint Conference on Artificial Intelligence*, page 3389–3396. AAAI Press, 2019. ISBN 9780999241141.
- [82] Xudong Shen, Chao Du, Tianyu Pang, Min Lin, Yongkang Wong, and Mohan Kankanhalli. Finetuning text-to-image diffusion models for fairness. In *The Twelfth International Conference on Learning Representations*, 2024. URL https://openreview.net/forum?id=hnrB5YHoYu.
- [83] Karen Simonyan and Andrew Zisserman. Very deep convolutional networks for large-scale image recognition. *CoRR*, abs/1409.1556, 2014. URL https://api.semanticscholar.org/CorpusID:14124313.
- [84] Jascha Sohl-Dickstein, Eric Weiss, Niru Maheswaranathan, and Surya Ganguli. Deep unsupervised learning using nonequilibrium thermodynamics. In *International Conference on Machine Learning*, pages 2256–2265. PMLR, 2015.
- [85] Yang Song, Jascha Sohl-Dickstein, Diederik P Kingma, Abhishek Kumar, Stefano Ermon, and Ben Poole. Score-based generative modeling through stochastic differential equations. In *International Conference on Learning Representations*, 2021. URL https://openreview.net/forum?id=PxTIG12RRHS.
- [86] Lukas Struppek, Dom Hintersdorf, Felix Friedrich, Patrick Schramowski, Kristian Kersting, et al. Exploiting cultural biases via homoglyphs in text-to-image synthesis. *Journal of Artificial Intelligence Research*, 78:1017–1068, 2023.
- [87] Christian Szegedy, Wojciech Zaremba, Ilya Sutskever, Joan Bruna, Dumitru Erhan, Ian Goodfellow, and Rob Fergus. Intriguing properties of neural networks, 2014. URL https://arxiv.org/abs/1312.6199.
- [88] Christian Szegedy, Wei Liu, Yangqing Jia, Pierre Sermanet, Scott Reed, Dragomir Anguelov, Dumitru Erhan, Vincent Vanhoucke, and Andrew Rabinovich. Going deeper with convolutions. In *Proceedings of the IEEE Conference on Computer Vision and Pattern Recognition*, pages 1–9, 2015.
- [89] Wei Ren Tan, Chee Seng Chan, Hernán E. Aguirre, and Kiyoshi Tanaka. Improved artgan for conditional synthesis of natural image and artwork. *IEEE Transactions on Image Processing*, 28(1):394–409, 2019. doi: 10.1109/TIP.2018.2866698.
- [90] Thanh Van Le, Hao Phung, Thuan Hoang Nguyen, Quan Dao, Ngoc N Tran, and Anh Tran. Anti-DreamBooth: Protecting users from personalized text-to-image synthesis. In *Proceedings of the IEEE/CVF International Conference on Computer Vision*, pages 2116–2127, 2023.

- [91] Gregory K Wallace. The JPEG still picture compression standard. *Communications of the ACM*, 34(4):30–44, 1991.
- [92] Hanhui Wang, Yihua Zhang, Ruizheng Bai, Yue Zhao, Sijia Liu, and Zhengzhong Tu. Edit away and my face will not stay: Personal biometric defense against malicious generative editing. *arXiv preprint arXiv:2411.16832*, 2024.
- [93] Yuxin Wen, John Kirchenbauer, Jonas Geiping, and Tom Goldstein. Tree-rings watermarks: Invisible fingerprints for diffusion images. In *Thirty-seventh Conference on Neural Information Processing Systems*, 2023. URL https://openreview.net/forum?id=Z57JrmubN1.
- [94] Haotian Xue and Yongxin Chen. Pixel is a barrier: Diffusion models are more adversarially robust than we think. *arXiv preprint arXiv:2404.13320*, 2024.
- [95] Haotian Xue, Alexandre Araujo, Bin Hu, and Yongxin Chen. Diffusion-based adversarial sample generation for improved stealthiness and controllability. In *Thirty-seventh Conference on Neural Information Processing Systems*, 2023. URL https://openreview.net/forum?id=JTwxy1P6U9.
- [96] Haotian Xue, Chumeng Liang, Xiaoyu Wu, and Yongxin Chen. Toward effective protection against diffusion-based mimicry through score distillation. In *The Twelfth International Conference on Learning Representations*, 2023.
- [97] Gong Zhang, Kai Wang, Xingqian Xu, Zhangyang Wang, and Humphrey Shi. Forget-menot: Learning to forget in text-to-image diffusion models. In *Proceedings of the IEEE/CVF Conference on Computer Vision and Pattern Recognition*, pages 1755–1764, 2024.
- [98] Kai Zhang, Lingbo Mo, Wenhu Chen, Huan Sun, and Yu Su. Magicbrush: A manually annotated dataset for instruction-guided image editing. In *Thirty-seventh Conference on Neural Information Processing Systems Datasets and Benchmarks Track*, 2023.
- [99] Richard Zhang, Phillip Isola, Alexei A Efros, Eli Shechtman, and Oliver Wang. The unreasonable effectiveness of deep features as a perceptual metric. In *Proceedings of the IEEE Conference on Computer Vision and Pattern Recognition*, pages 586–595, 2018.
- [100] Xuanyu Zhang, Runyi Li, Jiwen Yu, Youmin Xu, Weiqi Li, and Jian Zhang. EditGuard: Versatile image watermarking for tamper localization and copyright protection. In *Proceedings of the IEEE/CVF Conference on Computer Vision and Pattern Recognition*, pages 11964–11974, June 2024.
- [101] Yunqing Zhao, Tianyu Pang, Chao Du, Xiao Yang, Ngai-Man Cheung, and Min Lin. A recipe for watermarking diffusion models. *arXiv preprint arXiv:2303.10137*, 2023.
- [102] Zhengyue Zhao, Jinhao Duan, Kaidi Xu, Chenan Wang, Rui Zhang, Zidong Du, Qi Guo, and Xing Hu. Can protective perturbation safeguard personal data from being exploited by stable diffusion? In *Proceedings of the IEEE/CVF Conference on Computer Vision and Pattern Recognition*, pages 24398–24407, 2024.

A Discussions

A.1 Additional related work

Safety concerns in generative AI Aside from the image protection technique that we focus on in this paper, generative AI has introduced various new safety concerns and there has been increasing attention to address them from a technical perspective. For instance, a line of works focuses on *deepfake detection* [6, 41, 47, 50, 61], *i.e.*, developing methods to detect machine-generated ("fake") content within real-world data. Another possible approach is *watermarking* [20, 24, 54, 60, 93, 100, 101], which aims to embed a unique identifier into generated images, enabling the identification of the images or their creators. Focusing more on the modeling perspective, a series of works has aimed to fine-tune models to remove specific concepts [27, 28, 32, 42, 97], *e.g.*, nudity or certain image styles, ensuring that these concepts are excluded from generated content. Other works have focused on fairness and unbiased generation [19, 25, 82, 86], in an attempt to mitigate biases in generative models that may generate harmful stereotypes.

Adversarial examples for good Adversarial examples [5, 12, 87] were initially introduced to demonstrate that carefully crafted noise, imperceptible to human perception, can significantly change the outputs of machine learning models, causing them to make mistakes. Recent studies, however, have explored the potential of leveraging these adversarial examples for beneficial purposes, including robustifying classification models in imbalanced learning scenarios by generating synthetic minority class samples [39], enhancing model interpretability through counterfactual explanations, which illustrate minimal input changes needed to alter a model's prediction [36]. Notably, after the emergence of text-to-image diffusion models which can be easily misused for malicious purposes including deepfake, various studies [49, 77] have leveraged the adversarial examples against unauthorized editing facilitated by diffusion models.

A.2 Limitation and broader impact

Limitation A practical limitation of adversarial image protection is that, once an unprotected copy of an image is stolen and becomes publicly available, the perturbation can no longer effectively safeguard the image; an adversary can simply retrieve and edit the unprotected version. Consequently, future work could investigate model-level safeguards such as authorization systems that block unverified users from accessing the editing models, to prevent malicious editing at its source. Moreover, we note that the protective perturbation itself should not be regarded as a fundamental solution for manual editing scenarios by humans. While our approach may increase the cost of AI-based editing, it does not eliminate the threat posed by manual editing. Addressing such issues ultimately requires governance-level interventions beyond technical defenses.

Broader impact Protecting images with adversarial perturbations offers a practical benefit to AI safety by impeding unauthorized, harmful AI-based image edits. However, by demonstrating the vulnerability of existing protections, although it has already been noted by Hönig et al. [34], we might inadvertently encourage malicious users to abuse this vulnerability for unauthorized image editing. We therefore hope this work motivates future research that further strengthens existing protection frameworks, rather than inspiring adversaries to exploit purification tools.

B Overall Procedure: BlurGuard

```
Algorithm 1 BlurGuard
```

```
Input: source image x; noise budget \epsilon; # steps T_1, T_2; step size \gamma_1, \gamma_2; loss coefficient \lambda
Output: protected image \hat{\mathbf{x}}
  1: \{M_r\}_{r=1}^R \leftarrow \operatorname{SegmentAnything}(\mathbf{x})
2: Initialize \boldsymbol{\delta} \leftarrow \mathbf{0}
                                                                                                                      // Segment x into R binary masks using SAM
  3: for each region r \in \{1, \dots, R\} do
               Initialize \omega_r \leftarrow 0
                                                                                                                                                    // Parameterize the logarithm of \sigma
  5: end for
         {Stage 1: Optimize \omega}
  6: Initialize \delta_0 \sim \mathcal{N}(\mathbf{0}, \mathbf{I})
                                                                                                                   // Sample a Gaussian noise \delta_0 for optimizing \omega
  7: for each step t = 1, \ldots, T_1 do
             \begin{aligned} & \boldsymbol{\sigma} \leftarrow \exp(\boldsymbol{\omega}) \\ & \hat{\mathbf{x}} \leftarrow \mathbf{x} + \sum_{r=1}^{R} M_r \odot \mathcal{G}(\boldsymbol{\delta}_0, \sigma_r) \\ & \boldsymbol{\omega} \leftarrow \operatorname{Adam}(\boldsymbol{\omega}; L_{\operatorname{freq}}(\hat{\mathbf{x}}, \mathbf{x}), \gamma_1) \end{aligned} 
                                                                                                                  // Aggregate noises with blurring to construct \hat{\mathbf{x}}
10:
                                                                                                                                                                               // Update \omega via Adam
         {Stage 2: Optimize \delta}
12: for each step t = 1, \ldots, T_2 do
           \sigma \leftarrow \exp(\boldsymbol{\omega})

\hat{\mathbf{x}} \leftarrow \mathbf{x} + \sum_{r=1}^{R} M_r \odot \mathcal{G}(\boldsymbol{\delta}, \sigma_r) \\
L \leftarrow L_{\text{adv}}(\hat{\mathbf{x}}) + \lambda \cdot L_{\text{freq}}(\hat{\mathbf{x}}, \mathbf{x}) \\
\boldsymbol{\delta} \leftarrow \text{clip}(\boldsymbol{\delta} - \gamma_2 \cdot \frac{\nabla_{\boldsymbol{\delta}} L}{\|\nabla_{\boldsymbol{\delta}} L\|_2}; -\epsilon, \epsilon)

                                                                                                                                   // Adaptive blurring \delta with the learned \sigma
16:
                                                                                                                                 // Update \delta via PGD within noise budget \epsilon
17: end for
18: \hat{\mathbf{x}} \leftarrow \mathbf{x} + \sum_{r=1}^{R} M_r \odot \mathcal{G}(\boldsymbol{\delta}, \sigma_r)
19: return x
```

C Experimental Details

C.1 Evaluation metrics

To quantitatively evaluate our methods, we selected multiple metrics to assess various aspects of image quality and the effectiveness of image protection. For image quality, we selected metrics that focus on perceptual naturalness as well as structural integrity and pixel-level distortions. To evaluate protection performance, we used metrics to compare perceptual, structural, and pixel-level differences between generated images from protected and unprotected source images. Additionally, we selected metrics to measure whether their embeddings and distributions have significantly diverged.

LPIPS Learned Perceptual Image Patch Similarity (LPIPS) [99] measures the perceptual similarity between two images by comparing features extracted from a pre-trained neural network, such as VGG [83]. It focuses on high-level perceptual differences rather than pixel-wise accuracy.

SSIM Structural Similarity Index (SSIM) evaluates the structural similarity between two images, such as an original image \mathbf{X} and a transformed image \mathbf{Y} , by analyzing luminance (l), contrast (c), and structural patterns (s). It accounts for local pixel intensity patterns and combines these components into a single metric, defined as:

$$SSIM(\mathbf{X}, \mathbf{Y}) = [l(\mathbf{X}, \mathbf{Y})] \cdot [c(\mathbf{X}, \mathbf{Y})] \cdot [s(\mathbf{X}, \mathbf{Y})]. \tag{11}$$

PSNR Peak Signal-to-Noise Ratio (PSNR) assesses the similarity between two images, such as an original image x and a noised image y, by calculating the ratio between the maximum possible pixel intensity and the mean squared error (MSE). It provides a quantitative measure of how much the transformed image deviates from the original in terms of pixel-level fidelity, defined as:

$$PSNR(\mathbf{X}, \mathbf{Y}) = 20 \cdot \log_{10} \left(\frac{MAX(\mathbf{Y})}{\sqrt{MSE(\mathbf{X}, \mathbf{Y})}} \right).$$
 (12)

Image Alignment (IA) Score Image Alignment (IA) is a metric that measures the similarity between the embeddings of the source image and the protected image using cosine similarity. The embeddings are extracted using Contrastive Language-Image Pretraining (CLIP) [71], a pre-trained model that effectively captures high-level features from images by mapping them into an embedding space. The cosine similarity between the embeddings e_1 and e_2 of two images is defined as follows:

$$IA = \frac{\mathbf{e}_1 \cdot \mathbf{e}_2}{\|\mathbf{e}_1\| \|\mathbf{e}_2\|}.\tag{13}$$

FID Fréchet Inception Distance (FID) evaluates the difference between two image sets: a set of source images $\mathbb X$ and a set of images $\mathbb Y$. It quantifies the difference in feature distributions between the two sets by extracting features with a pre-trained Inception network [88] and modeling their distributions as multivariate Gaussians, characterized by means $(\mu_{\mathbb X}, \mu_{\mathbb Y})$ and covariances $(\Sigma_{\mathbb X}, \Sigma_{\mathbb Y})$. The FID is calculated as:

$$FID = ||\mu_{\mathbb{X}} - \mu_{\mathbb{Y}}||_{2}^{2} + Tr(\Sigma_{\mathbb{X}} + \Sigma_{\mathbb{Y}} - 2(\Sigma_{\mathbb{X}}\Sigma_{\mathbb{Y}})^{1/2}).$$

$$(14)$$

C.2 Implementation

Baselines For image protection baselines, we consider 4 baseline image protection methods: AdvDM [49], Mist [48], PhotoGuard [77], and SDS [96]. We set the noise budget $\epsilon=16/255$ and step size $\gamma=2/255$ for each iteration of PGD attack. For PhotoGuard, we used their encoder attack with no target image as it is the simplest adversarial objective that can be easily integrated with our framework.

To ensure a comprehensive evaluation, we also include additional baselines for specific tasks. For the inpainting task, we compare our framework with DiffusionGuard [18], using the same noise budget and step size as in other baselines. For the textual inversion task, we include Glaze [80] as an additional baseline.

Target models We use Stable Diffusion v1.4 [73] for image-to-image generation, textual inversion [26], and DreamBooth [74], while the inpainting model from Stable Diffusion v1.5 [73] is used for inpainting. For instruction-based editing, we use the pretrained InstructPix2Pix [7] model. For image-to-image generation and inpainting, we adopt the hyperparameter settings from PhotoGuard: 100 denoising steps, guidance scale of 7.5, and $\eta = 1$. For textual inversion, we follow the training and sampling procedures described in Hönig et al. [34]. For instruction-based editing, we apply the default hyperparameters provided in the InstructPix2Pix checkpoint on HuggingFace.⁷ For DreamBooth, we follow Anti-DreamBooth [90] for dataset sampling, training, and evaluation.

BlurGuard For constructing our protection, we optimized the logarithm of the Gaussian blur intensities $\log \sigma_1, \ldots, \log \sigma_R$ using the Adam optimizer with a learning rate (γ_1) of 0.1 during timesteps of $T_1 = 50$. After optimizing the blur intensities, we then optimize the adversarial perturbation with our 12-normalized PGD attack during timesteps of $T_2 = 100$ as same as other baseline protection methods. As the step size γ_2 for optimizing the perturbation δ , we used $\gamma_2 = 20$ for image-to-image generation and textual inversion task, and $\gamma_2 = 50$ for inpainting.

C.3 Datasets

ImageNet-Edit Image-to-image generation offers high accessibility compared to techniques such as inpainting or textual inversion, which require additional masks or model training. However, this accessibility also increases the risk of misuse, necessitating countermeasures. Currently, there is a lack of datasets for developing these countermeasures, hindering consistent and meaningful evaluations in concurrent research. From this perspective, we curated a benchmark dataset for image-to-image generation task which is a subset of ImageNet [21] including 80 carefully selected images of animals and objects paired with editing prompts as illustrated in figure 5. We selected these images based on the following criteria: (a) images containing 40% - 60% background, making it easy to edit both the background and the main object, and (b) square images close to a 512×512 resolution, as the backbone model (Stable Diffusion v1.4) is trained on this resolution. The editing prompts were generated by using ChatGPT [65] to generate captions based on the original images and then make minor modifications to these captions, such as replacing certain nouns or adjectives.

⁷https://huggingface.co/timbrooks/instruct-pix2pix



A white stork standing in a shallow wetland



A blue ceramic bowl filled with a salad



Junco bird perched on a snow-covered branch



Chesapeake Bay Retriever surrounded by blooming flowers in a garden.

Figure 5: Image-prompt pairs taken from ImageNet-Edit, a new benchmark dataset of 80 curated samples filtered from ImageNet, combined with ChatGPT for labeling, to evaluate image protection method in image-to-image generation task.

Helen For the inpainting task, we use the Helen dataset [44], following the pre-processing done by Cao et al. [10]. Specifically, they curated this dataset by sampling 80 images with the smallest face-to-image ratio to select images that are easy to modify. However, we found that the exact prompt set (used for editing) for this data is not publicly available; therefore we sample another set of prompts from the prompt set used by Choi et al. [18].

WikiArt We use the WikiArt dataset [89] for the textual inversion task. Each of the five artists (Albrecht Dürer, Edvard Munch, Alphonse Mucha, Edward Hopper, and Anna Ostroumova-Lebedeva) was selected based on [34], with 18 images assigned to each artist.

MagicBrush For the instruction-based editing task with InstructPix2Pix [7], we use the MagicBrush [98] dataset, which consists of images and corresponding instructions that can alter some aspects of the images. We randomly sampled 80 images and instructions from the test set of MagicBrush for our experiments.

VGGFace2 For the DreamBooth [74] tasks in Appendix D.1, we use the VGGFace2 [11] dataset, which is a large-scale face recognition dataset. Similar to the WikiArt dataset for the textual inversion task. For evaluation, we sample 50 identities in VGGFace2, following the experimental settings of Anti-DreamBooth [90].

C.4 Compute resources

We used a single NVIDIA A100 80GB GPU to run most of the experiments conducted; including processes of image protection, purification, and editing images. For fine-tuning Stable Diffusion models as done for the textual inversion experiments, we used a single NVIDIA RTX 3090 GPU, and a single NVIDIA RTX 3070 8GB to run Glaze.

C.5 Purification methods

We provide an overview of the seven noise purification methods considered in our experiments. These methods include not only those specifically trained for adversarial purification but also general image processing techniques that essentially work as a noise purifier.

JPEG compression JPEG compression [91] is an image compression standard for enhancing the efficiency of storing images. While this compression process utilizes Discrete Cosine Transform (DCT) quantization steps, some high-frequency details of an image can be suppressed by this compression.

Gaussian noise Adding Gaussian noise into an image itself can be a noise purification tool, but with image upscaling [62], Hönig et al. [34] claims that one can effectively purify the adversarial noise without degradation in image quality. We also consider Gaussian noise with upscaling as one of our purification tools.

Image upscaling Upscaling is a process that increases the resolution of an image by interpolating additional pixels. It can be used as a noise purification because resampling smooths high-frequency components, making it an effective tool for mitigating adversarial noise. An effective approach is to apply upscaling after performing JPEG compression or adding Gaussian noise, as these methods help suppress or disrupt adversarial patterns before the resampling step. Following this principle, we adopt both upscaling strategies as part of our purification methods.

Impress IMPRESS [10] removes noise from protected images to ensure that they can reconstruct themselves when input into the diffusion model. Since protected images are visually very similar to the original images, the purified images are refined to retain similar visual characteristics to the protected images.

DiffPure DiffPure [63] utilizes SDEdit [58], a purification method based on stochastic differential equations (SDE). DiffPure employs diffusion models for adversarial purification, effectively removing adversarial perturbations and recovering the original image. This process involves adding an appropriate level of noise during the forward diffusion step to neutralize adversarial patterns, followed by a reverse diffusion step to reconstruct a clean image.

GrIDPure GrIDPure [102] is an extension of DiffPure [63]. It utilizes a grid-based slicing and merging process by dividing high-resolution images into overlapping grids, purifying each grid using the diffusion model, and then merging them back together.

PDM-Pure PDM-Pure [94] is an adversarial purification method leveraging Pixel-Space Diffusion Models (PDM). It builds on SDEdit[58] by adding a small amount of noise to protected images and then performing a denoising process to remove protective patterns and restore the image closer to its original form.

D Additional Experiments

D.1 More editing scenarios

Naturalness				Worst-case Effectiveness					
Method	LPIPS ↓	SSIM ↑	PSNR ↑	FID ↑	LPIPS ↑	SSIM ↓	PSNR↓	IA ↓	
PhotoGuard [77]	0.25 ± 0.12	0.77 ± 0.08	28.1 ± 0.23	177.18	0.58 ± 0.08	0.25 ± 0.10	28.4 ± 0.44	0.89 ± 0.05	
AdvDM [49]	0.26 ± 0.11	0.80 ± 0.06	28.8 ± 0.28	176.74	0.61 ± 0.09	$\overline{0.23\pm0.09}$	28.4 ± 0.42	0.88 ± 0.04	
Mist [48]	0.24 ± 0.12	0.78 ± 0.07	28.7 ± 0.23	194.00	0.61 ± 0.08	0.23 ± 0.09	28.4 ± 0.43	0.88 ± 0.04	
SDS [96]	0.22 ± 0.10	0.80 ± 0.06	29.0 ± 0.37	176.89	0.57 ± 0.08	0.26 ± 0.10	28.4 ± 0.39	0.89 ± 0.05	
Glaze [80]	$\boldsymbol{0.14 \pm 0.09}$	0.90 ± 0.04	31.2 ± 0.42	169.80	0.57 ± 0.09	0.25 ± 0.09	28.5 ± 0.51	0.90 ± 0.04	
BlurGuard (Ours)	0.15 ± 0.08	0.97 ± 0.03	32.1 ± 3.06	181.89	0.59 ± 0.08	0.25 ± 0.10	28.3 ± 0.46	$\boldsymbol{0.87 \pm 0.05}$	

Table 8: Results on textual inversion with Stable Diffusion v1.4, under ℓ_{∞} protection within $\epsilon = \frac{16}{255}$. *Naturalness* indicates how imperceptible the protection is. *Worst-case effectiveness* is measured after applying 7 different noise purification methods to the protected image, representing the robustness of each protection method. The best is highlighted in **bold**, while the second-best is underlined.

Textual inversion Textual inversion [26] enables users to associate new visual concepts or styles into unique tokens via prompt tuning. However, it risks replicating copyrighted artwork and threatening intellectual property rights. We employed the WikiArt dataset [89], preprocessed as described in [34] to evaluate the performance of each protection methods. We fine-tune a text-to-image diffusion model on an image set $\mathbb X$ representing style using training steps = 2000, batch size = 4, and learning rate = 5×10^{-6} , following [34]. For each image $\mathbf x$, we generate a corresponding prompt $P_{\mathbf x} = C_{\mathbf x}$ + "by artist", where the image caption $C_{\mathbf x}$ is obtained using the BLIP-2 model [46]. The fine-tuned model generates images with a resolution of 768×768 using the DPM-Solver++ (2M) Karras scheduler [38, 53] over 50 sampling steps.

The results shows that BlurGuard surpassing most baselines in worst-case protection performance while maintaining superior image quality. Notably, BlurGuard achieves an LPIPS imperceptibility comparable to Glaze [80], which is explicitly optimized for minimizing LPIPS. Considering the inherent trade-off between imperceptibility and protection effectiveness, this substantially high imperceptibility suggests the potential for higher protection effectiveness while maintaining a similar level of imperceptibility to the baselines when a larger perturbation budget ϵ is used. This strong performance stems from our per-region blurring scheme, which adaptively incorporates textural information from images with diverse patterns. Given that the artworks used in textual inversion tasks often contain rich textures and vibrant colors, as shown in Figure 15, the high imperceptibility achieved by our method in these tasks is particularly meaningful.

DreamBooth We also compared BlurGuard with other protection baselines on DreamBooth, which fine-tunes a diffusion model so that the generated images depict a user-specified concept. We used VGGFace2 [11] dataset to fine-tune Stable Diffusion v1.4. For the baselines, we employed Anti-DreamBooth [90] and High-Frequency Anti-DreamBooth [64], which are specially designed frameworks to protect images against DreamBooth. Table 9 demonstrates that BlurGuard surpasses other protection methods including High-Frequency Anti-DreamBooth, which selectively applies large amount of perturbation only in high-frequency areas of the image. Moreover, the results show that BlurGuard can also be combined with other protection methods as a plug-and-play manner, supporting its high applicability.

Method	LPIPS ↑	FID ↑	SSIM ↓	PSNR↓	IA ↓
Anti-DreamBooth [90] High-Frequency Anti-DreamBooth [64]	$\begin{array}{c} 0.12 \pm 0.02 \\ 0.12 \pm 0.05 \end{array}$	127.93 138.45	$\frac{0.51 \pm 0.11}{0.53 \pm 0.10}$	$\frac{28.5 \pm 0.47}{28.6 \pm 0.43}$	$\frac{0.88 \pm 0.06}{0.89 \pm 0.05}$
BlurGuard + Anti-DreamBooth	0.12 ± 0.10	145.75	$\textbf{0.49} \pm \textbf{0.10}$	$\textbf{28.3} \pm \textbf{0.35}$	$\textbf{0.86} \pm \textbf{0.06}$

Table 9: Worst-case effectiveness of different image protection methods on Dreambooth, under ℓ_{∞} protection within $\epsilon = \frac{16}{255}$. Worst-case effectiveness is measured after applying 7 different noise-purification methods. The best value is in **bold**, the second-best is underlined.

D.2 Black-box transfer

IN-Edit ($\varepsilon = \frac{16}{255}$)	$\frac{16}{55}$) (a) SD-v1.4 \rightarrow SD-v3.5				(b) SD-v1.4 → FLUX.1-dev					
Method	FID ↑	LPIPS ↑	SSIM ↓	PSNR↓	IA↓	FID ↑	LPIPS ↑	SSIM↓	PSNR↓	IA↓
PhotoGuard [77] AdvDM [49]	112.58 98.25	0.40 ± 0.09 0.34 ± 0.10	0.48 ± 0.18 0.71 ± 0.09	29.1 ± 0.85 29.9 ± 1.04	0.90 ± 0.04 0.92 ± 0.04	72.60 71.74	0.26 ± 0.08 0.26 ± 0.08	0.80 ± 0.07 0.78 ± 0.06	30.7 ± 0.95 30.6 ± 1.06	0.95 ± 0.03 0.94 ± 0.04
Mist [48] SDS [96]	120.17 102.12	$\begin{array}{c} 0.43 \pm 0.08 \\ 0.41 \pm 0.09 \end{array}$	$\begin{array}{c} 0.47 \pm 0.19 \\ 0.52 \pm 0.14 \end{array}$	$\frac{28.8 \pm 0.83}{29.4 \pm 0.88}$	$\frac{0.89 \pm 0.05}{0.89 \pm 0.05}$	63.59 58.59	$\begin{array}{c} 0.21 \pm 0.06 \\ 0.19 \pm 0.06 \end{array}$	$\begin{array}{c} 0.80 \pm 0.06 \\ 0.81 \pm 0.07 \end{array}$	$\frac{30.3 \pm 0.87}{31.0 \pm 1.37}$	0.95 ± 0.03 0.96 ± 0.03
BlurGuard (Ours)	117.71	0.46 ± 0.08	$\boldsymbol{0.46 \pm 0.19}$	28.4 ± 0.54	0.88 ± 0.05	74.34	0.26 ± 0.09	0.79 ± 0.09	29.0 ± 0.69	0.93 ± 0.04

Table 10: Comparison of worst-case effectiveness on ImageNet- Edit for black-box transfer. We consider two additional scenarios (a) SD-v1.4 \rightarrow SD-v3.5 and (b) SD-v1.4 \rightarrow FLUX.1-dev. The best is highlighted in **bold**, while the second-best is underlined.

SD-v1.4 → SimSwap		Naturalness		Worst-case Effectiveness						
Method	LPIPS ↓	SSIM ↑	PSNR ↑	FID ↑	LPIPS ↑	SSIM ↓	PSNR↓	IA ↓		
PhotoGuard [77]	0.04 ± 0.02	0.96 ± 0.02	38.2 ± 2.53	18.34	$\boldsymbol{0.03 \pm 0.02}$	0.97 ± 0.02	40.0 ± 2.67	0.99 ± 0.00		
AdvDM [49]	0.04 ± 0.03	0.97 ± 0.01	40.7 ± 2.65	17.16	$\boldsymbol{0.03 \pm 0.02}$	0.97 ± 0.01	40.4 ± 2.43	0.99 ± 0.00		
Mist [48]	0.02 ± 0.01	0.98 ± 0.01	40.5 ± 2.60	14.10	0.02 ± 0.02	$\overline{0.98\pm0.01}$	41.0 ± 2.43	0.99 ± 0.00		
SDS [96]	0.06 ± 0.03	0.96 ± 0.02	38.9 ± 2.55	25.11	$\overline{0.03\pm0.02}$	0.97 ± 0.02	39.3 ± 2.44	0.99 ± 0.01		
DiffusionGuard [18]	0.04 ± 0.02	0.97 ± 0.01	39.6 ± 2.49	17.39	0.02 ± 0.02	0.97 ± 0.01	40.2 ± 2.33	0.99 ± 0.00		
BlurGuard (Ours)	0.03 ± 0.02	$\boldsymbol{0.99 \pm 0.01}$	38.7 ± 2.22	31.54	0.03 ± 0.01	$\boldsymbol{0.98 \pm 0.01}$	38.4 ± 2.37	$\boldsymbol{0.97 \pm 0.02}$		

Table 11: Black-box transfer on InpaintGuardBench for inpainting (SD-v1.4 \rightarrow SimSwap), under ℓ_{∞} protection within $\epsilon = \frac{16}{255}$. The best is highlighted in **bold**, while the second-best is <u>underlined</u>.

Transferability across diffusion models We further examine the black-box transferability of BlurGuard by evaluating its performance when adversarial protections from SD-v1.4 are transferred to newer diffusion models, including SD-v3.5 and FLUX.1-dev [43]. Note that these target models use the MMDiT architecture with flow-matching, which substantially differ from SD-v1.4. As shown in Table 10, BlurGuard consistently improves performance over PhotoGuard across all metrics, demonstrating its clear advantage in enhancing transferability. Moreover, BlurGuard maintains strong and competitive protection performance across all target models, highlighting the general applicability of our framework to diverse generative architectures. These results show that BlurGuard offers a broadly transferable solution for adversarial image protection in diffusion-based models.

Transferability to GAN To examine the cross-framework transferability of BlurGuard, we conduct a black-box transfer experiment from SD-v1.4 to SimSwap [14], a GAN-based method for deepfake generation. We perform the evaluation on the human portrait subset of InpaintGuardBench [18]. As shown in Table 11, BlurGuard maintains strong performance in both naturalness and worst-case effectiveness, confirming that the protective perturbations generated by our framework remain effective even when transferred across fundamentally different generative frameworks from diffusion models to GANs. These results highlight the robustness and broad generalizability of BlurGuard beyond diffusion-based architectures.

D.3 Evaluation with other diffusion models

SD-v2.1 ($\varepsilon = \frac{16}{255}$)		Naturalness		Worst-case Effectiveness						
Method	LPIPS ↓	SSIM ↑	PSNR ↑	FID ↑	LPIPS ↑	SSIM ↓	PSNR↓	IA ↓		
PhotoGuard [77]	0.34 ± 0.11	0.70 ± 0.11	28.2 ± 0.32	145.29	0.36 ± 0.07	0.66 ± 0.12	29.4 ± 0.85	0.91 ± 0.04		
AdvDM [49]	0.25 ± 0.10	0.79 ± 0.09	29.4 ± 0.33	$\overline{140.76}$	0.35 ± 0.07	0.67 ± 0.12	29.7 ± 0.96	0.91 ± 0.04		
Mist [48]	0.31 ± 0.12	0.75 ± 0.09	28.9 ± 0.25	143.37	0.38 ± 0.07	0.66 ± 0.12	29.6 ± 0.91	0.90 ± 0.04		
SDS [96]	0.32 ± 0.11	0.79 ± 0.08	29.8 ± 0.57	136.36	0.36 ± 0.08	0.67 ± 0.12	29.7 ± 1.00	0.91 ± 0.04		
BlurGuard (Ours)	$\textbf{0.22} \pm \textbf{0.10}$	0.93 ± 0.09	31.1 ± 2.27	154.46	0.41 ± 0.07	0.62 ± 0.11	28.7 ± 0.55	0.89 ± 0.04		

Table 12: Results on image-to-image generation with SD-v2.1, under ℓ_{∞} protection within $\epsilon = \frac{16}{255}$. Naturalness indicates how imperceptible the protection is. Worst-case effectiveness is measured after applying 7 different noise purification methods to the protected image, representing the robustness of each protection method. The best is highlighted in **bold**, while the second-best is underlined.

SD-v3.5 ($\varepsilon = \frac{16}{255}$)		Naturalness		Worst-case Effectiveness						
Method	LPIPS ↓	SSIM ↑	PSNR ↑	FID ↑	LPIPS ↑	SSIM ↓	PSNR↓	IA↓		
PhotoGuard [77]	$\textbf{0.24} \pm \textbf{0.09}$	0.79 ± 0.09	31.5 ± 1.30	121.58	0.45 ± 0.08	0.48 ± 0.19	28.6 ± 0.64	0.88 ± 0.05		
AdvDM [49]	0.28 ± 0.10	0.77 ± 0.08	29.5 ± 0.26	$\overline{116.36}$	0.42 ± 0.08	0.48 ± 0.19	29.0 ± 0.94	0.89 ± 0.05		
Mist [48]	0.25 ± 0.09	0.80 ± 0.09	30.9 ± 1.14	118.91	0.45 ± 0.08	0.48 ± 0.19	28.6 ± 0.64	$\overline{0.88 \pm 0.05}$		
SDS [96]	0.25 ± 0.11	$\underline{0.86 \pm 0.08}$	29.5 ± 0.32	119.20	0.46 ± 0.08	0.47 ± 0.19	28.5 ± 0.56	0.88 ± 0.05		
BlurGuard (Ours)	0.25 ± 0.10	$\boldsymbol{0.88 \pm 0.13}$	30.4 ± 1.97	125.32	$\boldsymbol{0.48 \pm 0.07}$	$\boldsymbol{0.46 \pm 0.18}$	28.4 ± 0.46	$\boldsymbol{0.88 \pm 0.05}$		

Table 13: Results on image-to-image generation with SD-v3.5, under ℓ_{∞} protection within $\epsilon = \frac{16}{255}$. Naturalness indicates how imperceptible the protection is. Worst-case effectiveness is measured after applying 7 different noise purification methods to the protected image, representing the robustness of each protection method. The best is highlighted in **bold**, while the second-best is underlined.

FLUX.1-dev ($\varepsilon = \frac{16}{255}$)		Naturalness		Worst-case Effectiveness						
Method	LPIPS ↓	SSIM ↑	PSNR ↑	FID ↑	LPIPS ↑	SSIM ↓	PSNR↓	IA↓		
PhotoGuard [77]	0.21 ± 0.10	0.86 ± 0.07	32.1 ± 0.33	80.22	0.28 ± 0.06	0.68 ± 0.11	29.5 ± 0.31	0.91 ± 0.05		
AdvDM [49]	0.27 ± 0.10	0.85 ± 0.07	32.6 ± 1.10	83.42	0.28 ± 0.06	0.68 ± 0.12	28.8 ± 0.72	0.90 ± 0.05		
Mist [48]	0.26 ± 0.09	0.87 ± 0.08	32.3 ± 1.40	84.10	0.29 ± 0.07	0.67 ± 0.12	29.7 ± 0.60	0.90 ± 0.04		
SDS [96]	0.24 ± 0.10	$\underline{0.88 \pm 0.08}$	32.2 ± 0.80	81.65	0.28 ± 0.06	0.68 ± 0.11	28.6 ± 0.48	0.90 ± 0.05		
BlurGuard (Ours)	0.23 ± 0.11	$\boldsymbol{0.89 \pm 0.07}$	33.4 ± 2.90	85.21	0.30 ± 0.10	0.67 ± 0.13	28.4 ± 0.33	0.89 ± 0.05		

Table 14: Results on image-to-image generation with FLUX.1-dev, under ℓ_{∞} protection within $\epsilon = \frac{16}{255}$. Naturalness indicates how imperceptible the protection is. Worst-case effectiveness is measured after applying 7 different noise purification methods to the protected image, representing the robustness of each protection method. The best is highlighted in **bold**, while the second-best is underlined.

We further investigate the generalizability of BlurGuard across more recent diffusion models by constructing protections against Stable Diffusion v2.1 (SD-v2.1), SD-v3.5, and FLUX.1-dev. In particular, SD-v3.5 and FLUX.1-dev adopt the MMDiT architecture with flow-matching training, representing a substantially different design paradigm from SD-v1.4 used in most of our experiments. As summarized in Tables 12, 13, and 14, BlurGuard consistently surpasses all baseline protection methods across nearly all metrics, demonstrating its robustness and scalability to newer, more advanced diffusion backbones. Figure 6 also supports these findings qualitatively.

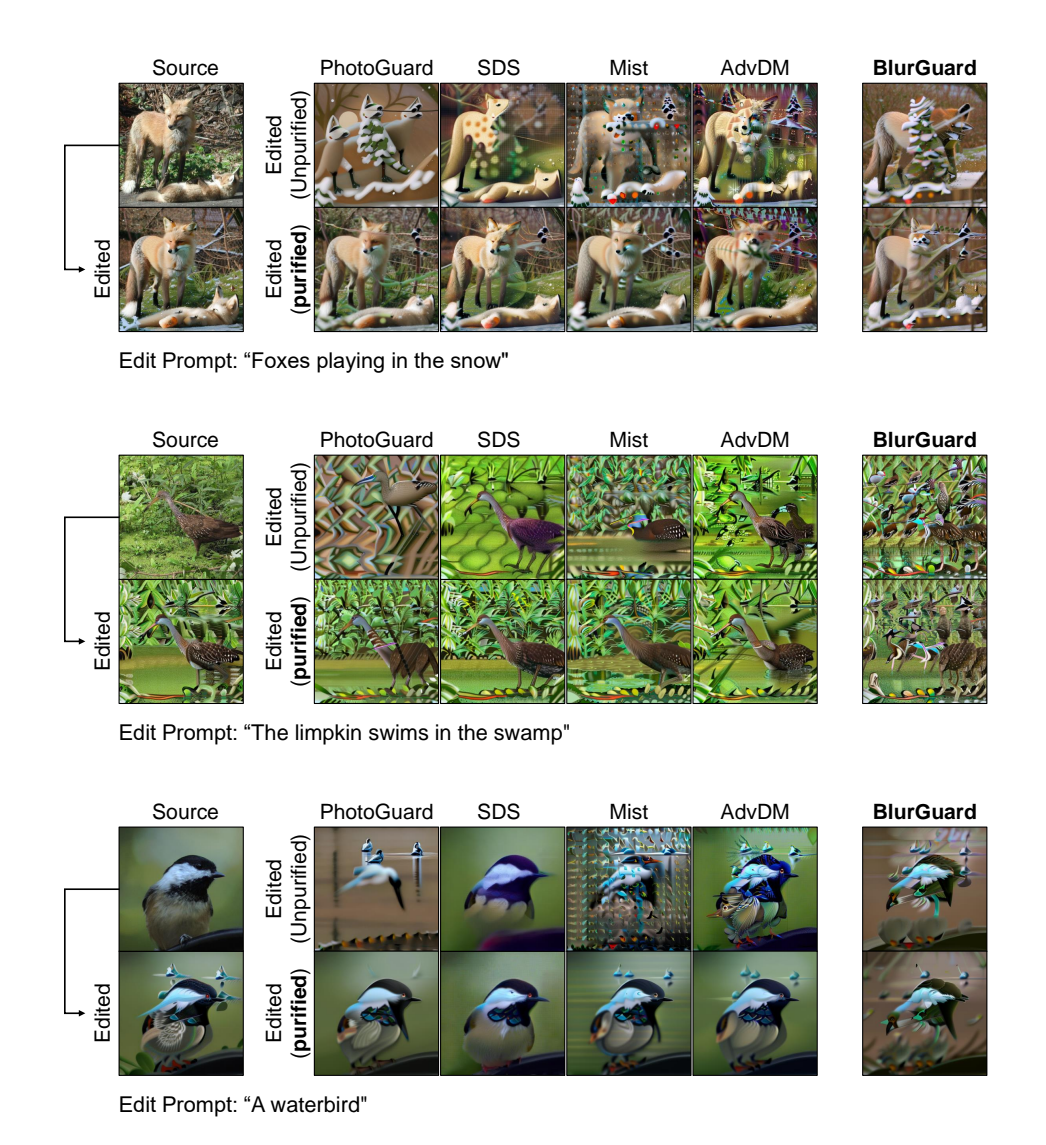


Figure 6: Qualitative comparison on image-to-image generation using Stable Diffusion v2.1.

D.4 Ablation study

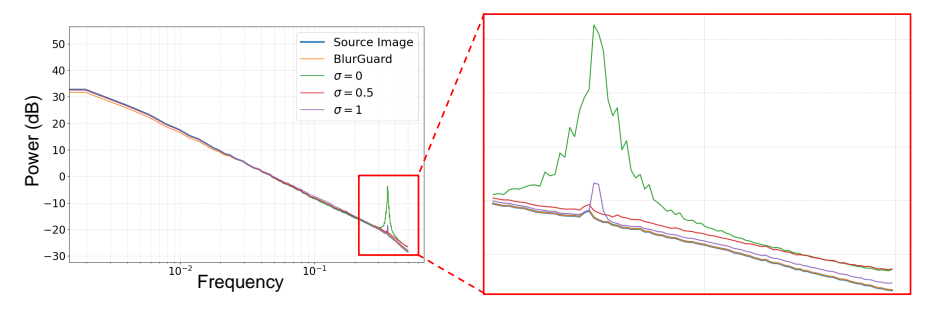
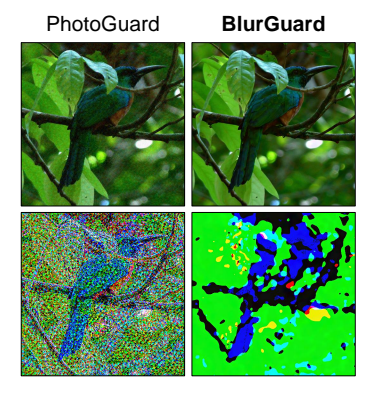


Figure 7: Comparison of the Radially-Averaged Power Spectral Density (RAPSD) of image protections using constant Gaussian blur intensity σ . The deviation in high-frequency bands (right side of the plot) often corresponds to the vulnerability against noise purification.

On the constant σ ablations We have shown that adaptive blurring is effective both for the naturalness and robustness of image protection (see Section 5.2). In Figure 7, we further show how the different blur intensities σ affect the frequency spectrum of protected images by showing their RAPSD. Unlike the original image that shows a linear RAPSD trend, protected images with non-blurred perturbation ($\sigma=0$) or perturbation with fixed blur intensity ($\sigma=0.5,1$) show large deviations in high-frequency levels. This deviation in high-frequency bands can directly harm the robustness of protection. These observations support the low protection performances shown by constant σ ablations ($\sigma=0.0,0.5,1.0$) reported in Table 6.



Visualization of perturbation We present a qualitative comparison of actual perturbations between PhotoGuard and our proposed BlurGuard in Figure 8; overall, we confirm that PhotoGuard tends

Figure 8: Visualization of the added noise from PhotoGuard and BlurGuard (ours).

to generate high-frequency perturbations uniformly across the image, whereas BlurGuard applies adaptive blurring per region, producing perturbations that are both more natural and harder to purify.

Lower perturbation budget We report the results on image-to-image task under ℓ_{∞} protection within $\epsilon = \frac{8}{255}$, which can be more practical when the perturbation is required to be merely perceptible. We show that BlurGuard also demonstrates its effectiveness both in quantitative results in Table 15. While the PSNR naturalness of BlurGuard may appear slightly lower, this reflects a deliberate design choice rather than higher perceptibility. PSNR focuses on pixel-wise fidelity rather than perceptual similarity and often penalizes imperceptible local deviations. In contrast, BlurGuard intentionally allocates perturbations within perceptually insensitive regions through region-wise frequency adaptation, which can lower PSNR while preserving imperceptibility, as qualitatively illustrated in Figure 11.

IN-Edit ($\epsilon = \frac{8}{255}$)		Naturalness		Worst-case Effectiveness						
Method	LPIPS ↓	SSIM ↑	PSNR ↑	FID ↑	LPIPS ↑	SSIM ↓	PSNR ↓	IA ↓		
PhotoGuard [77]	0.06 ± 0.04	0.89 ± 0.05	32.4 ± 0.38	57.31	0.14 ± 0.06	0.83 ± 0.06	31.6 ± 1.25	0.97 ± 0.03		
AdvDM [49]	0.14 ± 0.07	0.88 ± 0.05	32.6 ± 0.50	83.31	$\boldsymbol{0.24 \pm 0.06}$	$\boldsymbol{0.76 \pm 0.08}$	30.6 ± 1.30	0.95 ± 0.03		
Mist [48]	0.12 ± 0.05	0.86 ± 0.06	32.0 ± 0.45	73.21	0.21 ± 0.07	0.77 ± 0.08	30.6 ± 1.18	0.95 ± 0.03		
SDS [96]	0.09 ± 0.03	0.87 ± 0.06	32.9 ± 0.54	71.28	0.19 ± 0.06	$\overline{0.79 \pm 0.08}$	$\overline{30.9 \pm 1.28}$	0.96 ± 0.03		
BlurGuard (Ours)	0.08 ± 0.05	$\boldsymbol{0.95 \pm 0.07}$	30.7 ± 0.46	84.38	0.23 ± 0.08	0.77 ± 0.08	29.9 ± 0.89	0.94 ± 0.04		

Table 15: Results on image-to-image generation with SD-v1.4, under ℓ_{∞} protection within $\epsilon = \frac{8}{255}$. Naturalness indicates how imperceptible the protection is. Worst-case effectiveness is measured after applying 7 different noise purification methods to the protected image, representing the robustness of each protection method. The best is highlighted in **bold**, while the second-best is <u>underlined</u>.

Lower image resolutions To reflect real-world scenarios where we often encounter variable image resolutions, we additionally evaluate BlurGuard at lower image resolutions, viz., 128×128 and 256×256 . For the evaluation, we down-sample the images in ImageNet-Edit dataset to each target resolution; the results are summarized in Table 16a and Table 16b. Interestingly, BlurGuard stands out as the only approach that could effectively preserve its effectiveness, whereas all the other considered baselines commonly suffer from significant degradation in worst-case effectiveness during the resampling procedure in handling different resolutions. These results underscore the utility of BlurGuard in a practical setup when input images differ from the 512×512 resolution on which the Stable Diffusion model is primarily trained.

IN-Edit ($\epsilon = \frac{16}{255}$)		Naturalness		Worst-case Effectiveness						
Method	LPIPS ↓	SSIM ↑	PSNR ↑	FID ↑	LPIPS ↑	SSIM ↓	PSNR↓	IA ↓		
PhotoGuard [77]	0.09 ± 0.06	0.81 ± 0.09	29.8 ± 0.57	70.88	0.07 ± 0.04	0.92 ± 0.03	32.2 ± 1.41	0.96 ± 0.03		
AdvDM [49]	$\boldsymbol{0.09 \pm 0.05}$	0.85 ± 0.08	29.3 ± 0.27	82.57	0.09 ± 0.04	0.91 ± 0.04	31.5 ± 0.99	0.96 ± 0.02		
Mist [48]	0.17 ± 0.07	0.78 ± 0.10	29.7 ± 0.62	118.35	0.12 ± 0.06	0.87 ± 0.05	30.3 ± 0.81	0.94 ± 0.03		
SDS [96]	$\underline{0.10 \pm 0.04}$	0.83 ± 0.08	29.6 ± 0.35	82.06	0.08 ± 0.04	0.91 ± 0.03	31.9 ± 1.39	0.96 ± 0.02		
BlurGuard (Ours)	0.10 ± 0.04	$\boldsymbol{0.92 \pm 0.08}$	32.5 ± 3.54	155.33	0.23 ± 0.08	$\boldsymbol{0.84 \pm 0.05}$	28.8 ± 0.56	0.90 ± 0.05		

(a) Results on 128×128 resolution.

IN-Edit ($\epsilon = \frac{16}{255}$)		Naturalness		Worst-case Effectiveness						
Method	LPIPS ↓	SSIM ↑	PSNR ↑	FID ↑	LPIPS ↑	SSIM ↓	PSNR↓	IA ↓		
PhotoGuard [77]	0.16 ± 0.08	0.75 ± 0.10	30.0 ± 0.60	73.80	0.13 ± 0.05	0.89 ± 0.04	31.8 ± 1.44	0.96 ± 0.03		
AdvDM [49]	0.15 ± 0.07	0.81 ± 0.09	29.4 ± 0.27	76.72	0.14 ± 0.05	0.88 ± 0.04	31.4 ± 1.33	0.96 ± 0.02		
Mist [48]	0.22 ± 0.08	0.75 ± 0.10	29.7 ± 0.45	96.34	0.16 ± 0.06	0.86 ± 0.05	30.6 ± 1.17	0.95 ± 0.03		
SDS [96]	0.17 ± 0.05	0.78 ± 0.08	29.4 ± 0.47	93.78	0.14 ± 0.05	0.87 ± 0.05	31.3 ± 1.47	$\underline{0.95 \pm 0.03}$		
BlurGuard (Ours)	0.13 ± 0.06	$\boldsymbol{0.92 \pm 0.09}$	31.8 ± 2.95	121.84	0.27 ± 0.09	0.81 ± 0.06	28.8 ± 0.57	0.92 ± 0.04		

(b) Results on 256×256 resolution.

Table 16: Results of image-to-image generation on low-resolution inputs under ℓ_{∞} protection with $\epsilon = \frac{16}{255}$. Naturalness indicates how imperceptible the protection is. Worst-case effectiveness is measured after applying 7 different noise purification methods to the protected image. The best is highlighted in **bold**, while the second-best is underlined.

Adaptive blurring parameter Table 17 shows an ablation where we vary the SAM hyperparameter related to the number of masks that BlurGuard optimizes. Allowing more masks slightly lowers the naturalness but consistently improves worst-case effectiveness. This is likely because a higher number of masks enables a more flexible optimization in BlurGuard. However, removing adaptive blurring itself significantly degrades the protection, verifying its importance to BlurGuard.

IN-Edit ($\epsilon = \frac{16}{255}$)	Naturalness	Worst-case Effect.			
Method	SSIM ↑	FID ↑	LPIPS ↑		
w/o Per-region masks.	0.94	96.6	0.29		
Avg. $\#$ Masks = 10.3.	0.91	108.5	0.34		
Avg. # Masks = 21.4.	0.89	115.9	0.36		
Avg # Masks = 4.7 (Ours)	0.93	107.9	0.32		

Table 17: Additional ablation results on number of masks in adaptive blurring.

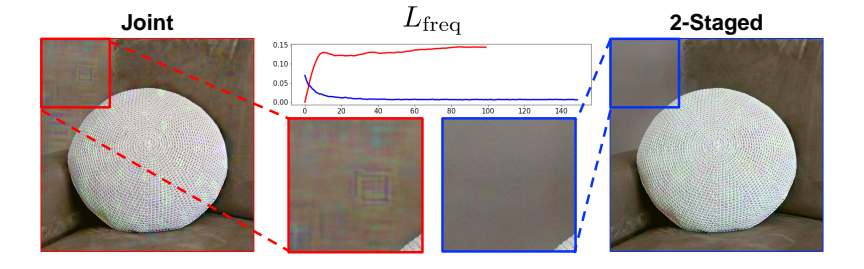


Figure 9: Ablation study on two-stage optimization of BlurGuard. Qualitative comparison between BlurGuard and its variant which jointly optimizes the blur intensities σ and the adversarial perturbation δ . We also report the trend of $L_{\rm freq}$ in each setting.

Two-stage optimization We also compare our two-stage optimization scheme with its ablation, *i.e.*, that jointly optimizes the two objectives $L_{\rm adv}$ and $L_{\rm freq}$. As observed in Figure 9, the two-stage optimization can help to stabilize the optimization of frequency loss $L_{\rm freq}$. In qualitative manner, on the other hand, we observe that the joint optimization (left) often generates unnatural artifacts with patterns in their protection; this happens when the frequency loss $L_{\rm freq}$ is minimized by tuning δ , rather than σ , making Gaussian blur less effective.

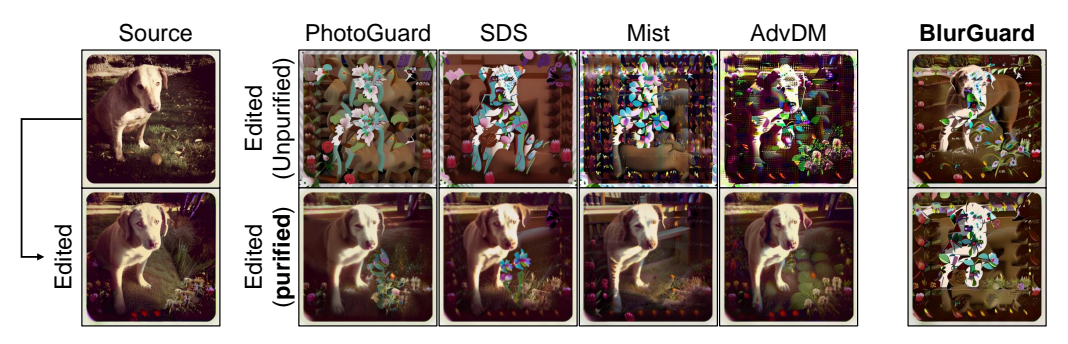
Detailed ablation on blurring design Note that BlurGuard applies adaptive blurring only to δ , not the entire image $\mathbf{x} + \delta$. To verify this adaptive blurring design as an effective way to control its frequency band, we compare BlurGuard with two frequency adaptation variants. Specifically, we apply (i) *global blurring* to the entire protected image $\mathbf{x} + \delta$, and (ii) *sharpening* to the perturbation δ using unsharp masking [68]. As shown in Table 18, these variants underperform BlurGuard in both naturalness and worst-case effectiveness of protection. Global blurring moderately improves robustness but shows a notable drop in SSIM and LPIPS naturalness metrics compared to BlurGuard, since blurring the entire image removes high-frequency details and thus compromises perceptual quality. The adaptive sharpening scheme fails to provide effective protection after purification because sharpening amplifies high-frequency components that are easily suppressed by existing purification techniques such as JPEG compression.

IN-Edit ($\varepsilon = \frac{16}{255}$)		Naturalness		Worst-case Effectiveness						
Method	LPIPS ↓	SSIM ↑	PSNR ↑	FID ↑	LPIPS ↑	SSIM ↓	PSNR↓	IA↓		
PhotoGuard [77]	0.34 ± 0.11	0.70 ± 0.11	28.2 ± 0.32	92.21	0.27 ± 0.07	0.73 ± 0.10	$\underline{29.9 \pm 1.07}$	$\underline{0.94 \pm 0.04}$		
$\mathbf{x} + \mathrm{Blur}(\boldsymbol{\delta})$	0.21 ± 0.10	0.93 ± 0.09	31.1 ± 2.29	107.88	0.32 ± 0.09	0.70 ± 0.09	28.8 ± 0.42	0.92 ± 0.05		
$Blur(\mathbf{x} + \boldsymbol{\delta})$	0.32 ± 0.11	0.79 ± 0.08	32.3 ± 1.11	98.45	0.30 ± 0.07	0.71 ± 0.10	30.1 ± 1.21	0.94 ± 0.04		
$\operatorname{Sharpen}(\boldsymbol{\delta})$	0.35 ± 0.12	0.65 ± 0.10	30.9 ± 1.08	82.72	$\overline{0.28 \pm 0.08}$	$\overline{0.72 \pm 0.10}$	30.4 ± 1.38	0.94 ± 0.04		

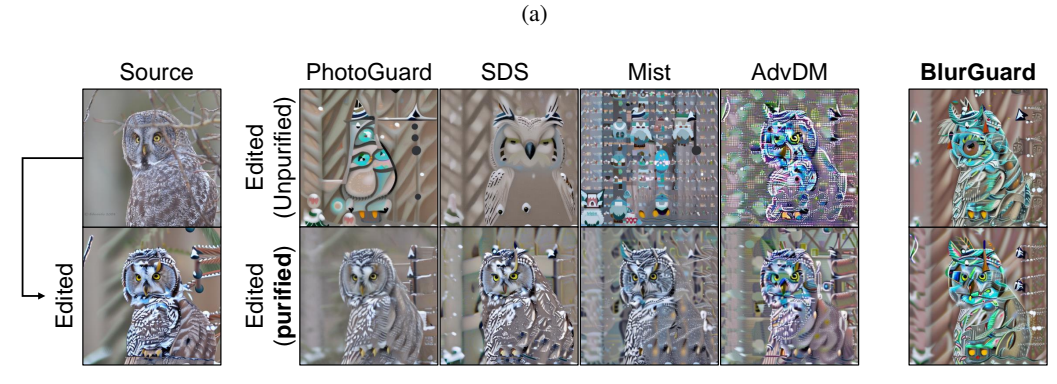
Table 18: Comparison of BlurGuard with additional blurring design ablations.

E Additional Qualitative Results

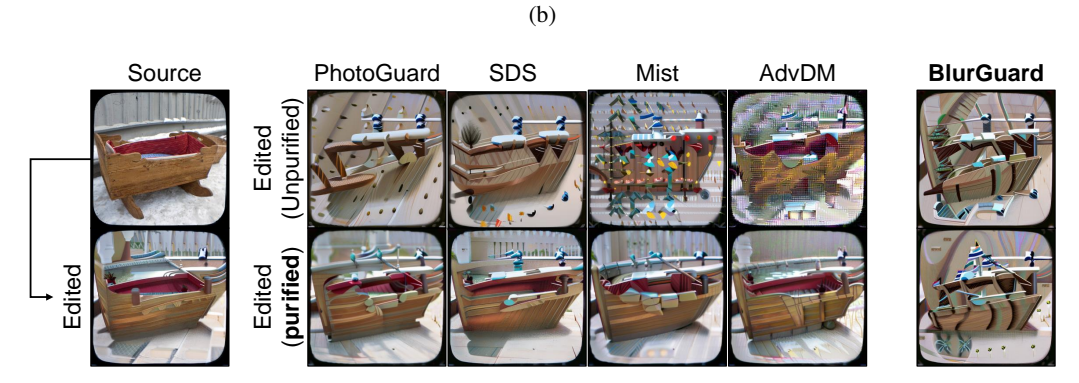
In this section, we report additional qualitative results of our proposed method, BlurGuard, to further support its effectiveness. In Figure 10, we report additional qualitative results on the black-box transfer experiments (Section 5.1). Figure 12, Figure 14, and Figure 15 compares BlurGuard with other baselines in image-to-image generation, inpainting, and textual inversion tasks, respectively. Figure 6 supplies qualitative results on the Stable Diffusion v2.1 model (Appendix D.3).



Edit Prompt: "Chesapeake Bay Retriever surrounded by blooming flowers in a garden"



Edit Prompt: "An owl on a snowy day"



Edit Prompt: "A wooden ship by the pool"

Figure 10: Qualitative comparison on black-box transfer, where each protection is crafted using SD-v1.4 and tested on SD-v2.1.

(c)

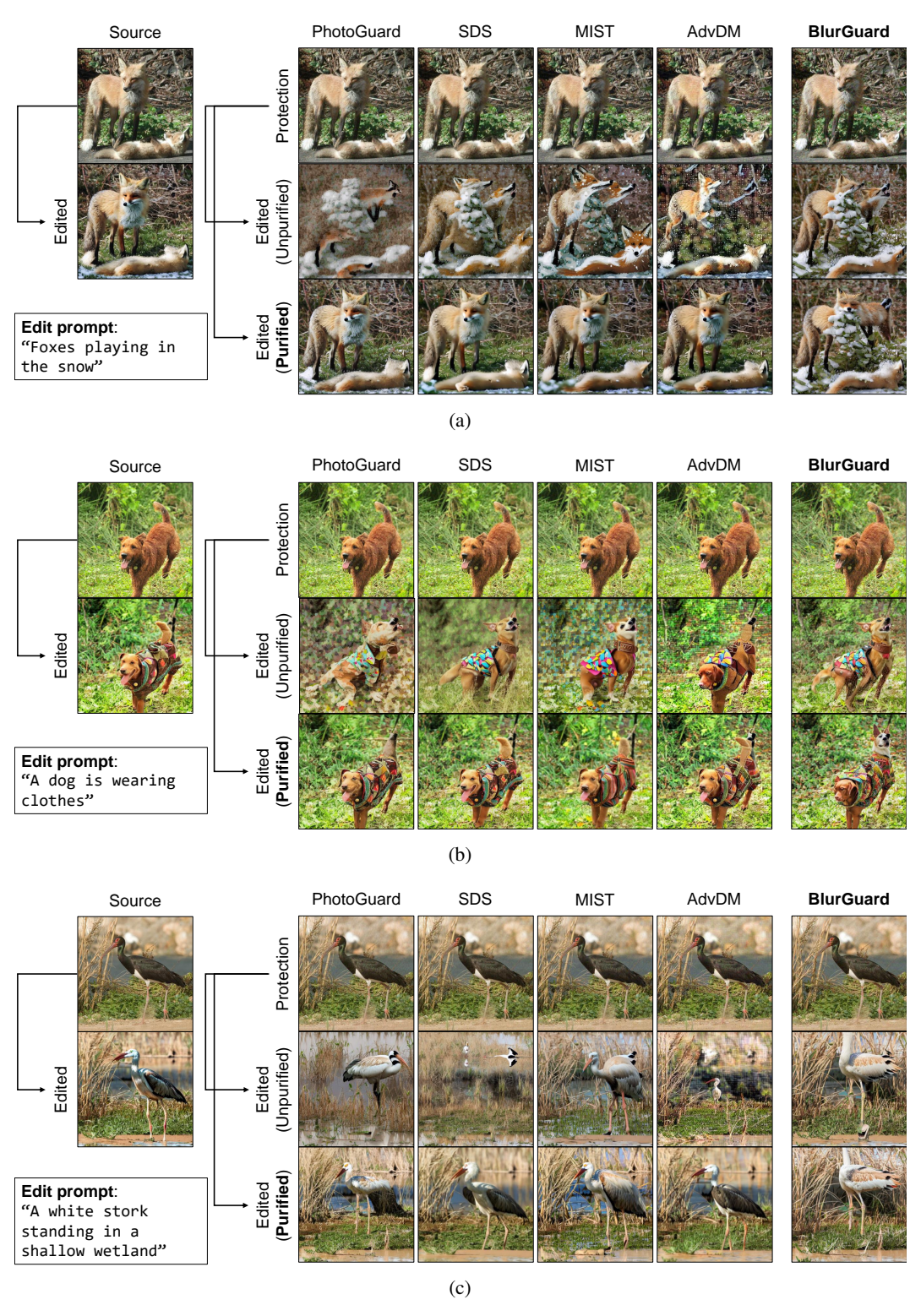


Figure 11: Qualitative results on image-to-image generation under ℓ_{∞} protection within $\epsilon=\frac{8}{255}$. While all baselines fail to protect the image after purification, only BlurGuard remains robust after purification, generating unrealistic images.

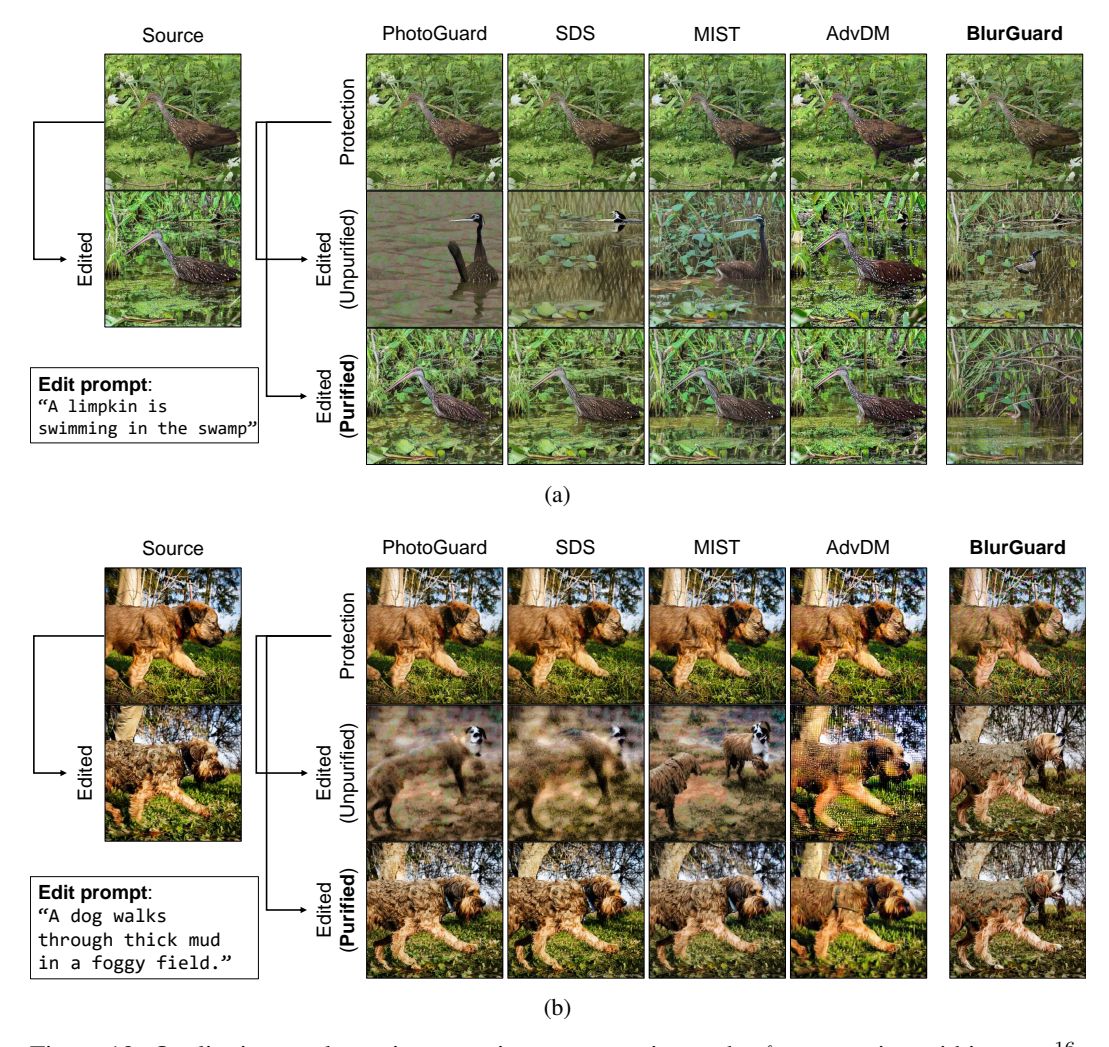
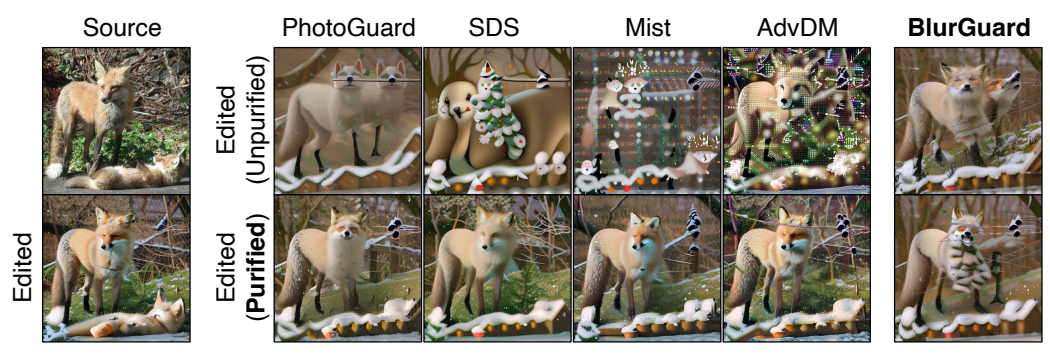


Figure 12: Qualitative results on image-to-image generation under ℓ_{∞} protection within $\epsilon=\frac{16}{255}$. While all baselines fail to protect the image after purification, only BlurGuard remains robust after purification, generating unrealistic images.



Edit Prompt: "Foxes playing in the snow"

Figure 13: Qualitative comparison of black-box transfer under ℓ_{∞} protection within $\epsilon=\frac{16}{255}$, where each protection is crafted using SD-v1.4 while tested to SD-v2.1.

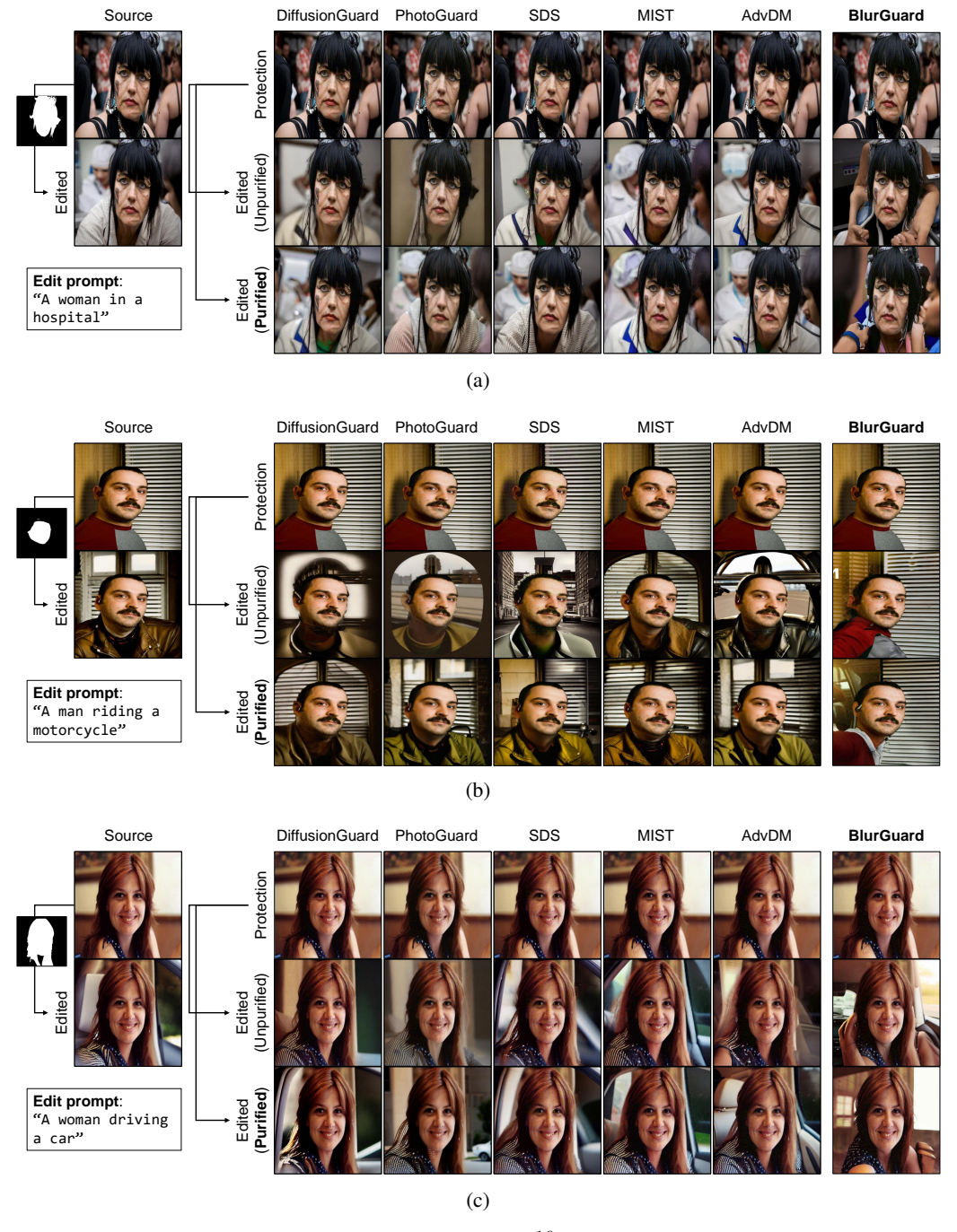


Figure 14: Qualitative inpainting results within $\epsilon=\frac{16}{255}$. Baselines are eventually purified and produce realistic edits, whereas BlurGuard disrupts inpainting.

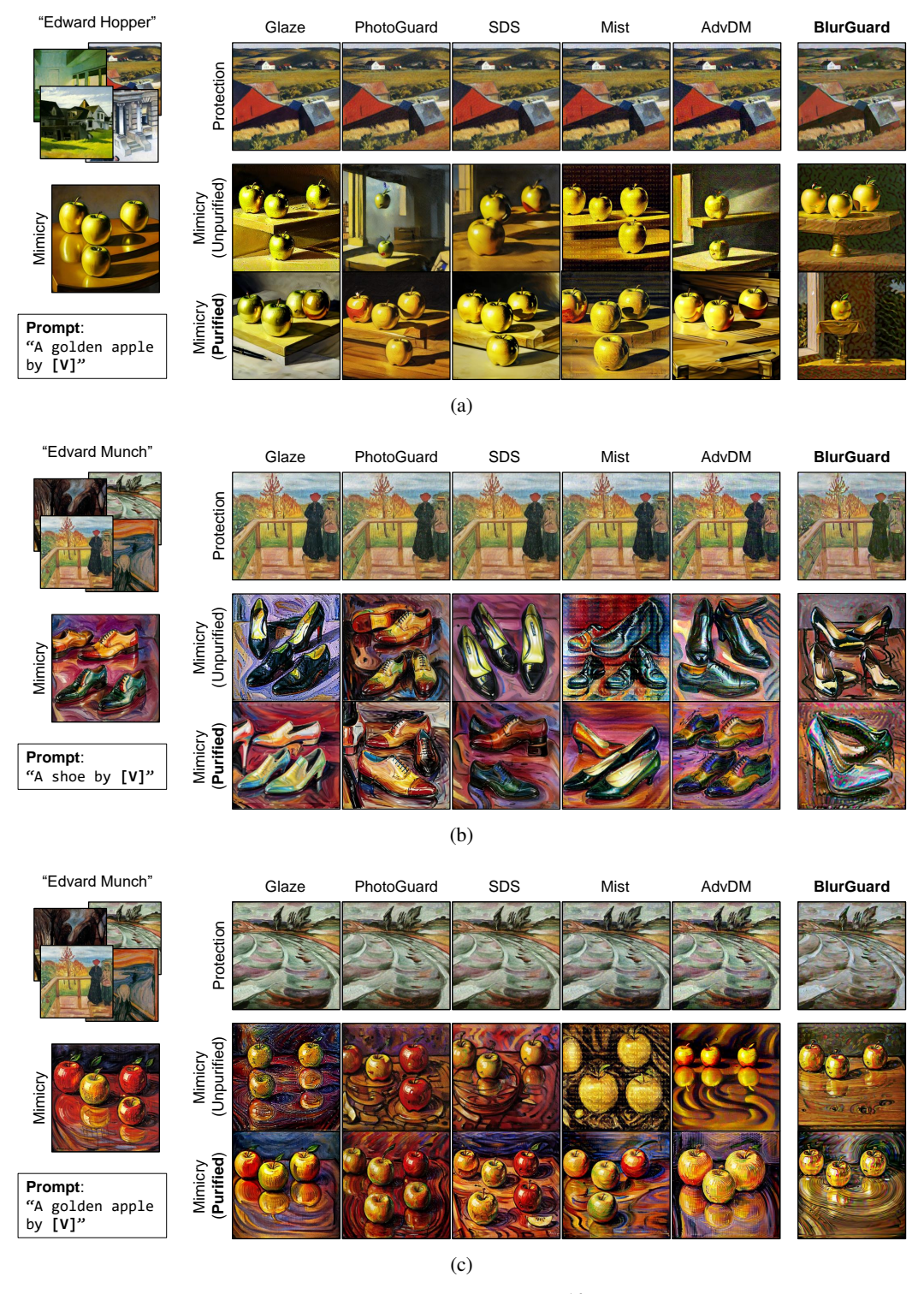
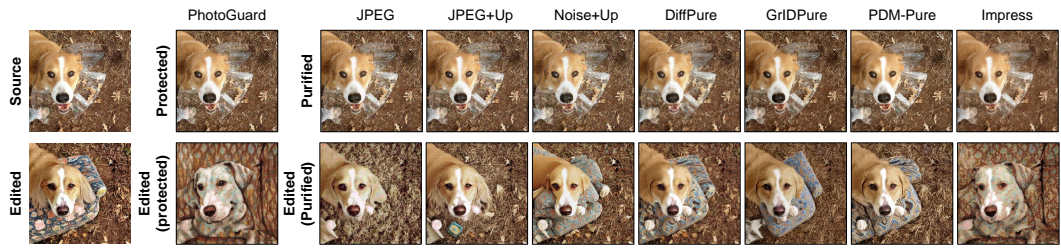


Figure 15: Qualitative results on textual inversion within $\epsilon=\frac{16}{255}$. BlurGuard introduces artifacts that block style extraction; baselines allow near-identical styles.

F Individual Effects of Tested Purifications



Edit prompt: "A dog sitting on a blue couch"

Figure 16: Qualitative examples of various purified images and the corresponding generated images after applying PhotoGuard protection. The notation "Up" indicates upscaling.

Following our definition of worst-case effectiveness, we test seven different purification methods (viz., as shown in Figure 16) per sample and select the result that deviated the least from the original edited image. Here, we present the detailed results of each noise purification method. Specifically, we evaluate across all eight cases: when each of the seven purification methods is applied individually and when no purification is applied. Table 19 presents the detailed results for the image-to-image generation task, Table 20 corresponds to the inpainting task, and Table 21 reports the results for the textual inversion task.

Although all baseline protections are readily bypassed by the purification tools we evaluate, BlurGuard remains robust against each one of them. Furthermore, we observed that the protection effectiveness of BlurGuard occasionally increases after purification, as reported in Table 19, Table 20, and Table 21. This counterintuitive observation emphasizes the resilience of BlurGuard to existing purification techniques. Since BlurGuard relies minimally on high-frequency components as shown in Figure 2a and Figure 8, purification methods that aggressively suppress high frequencies can cause the purified image to deviate further from the source image as illustrated in Figure 2b.

			Before Purific	ation				Noise + Upsca	aling	
Method	FID ↑	LPIPS ↑	SSIM ↓	PSNR↓	IA ↓	FID ↑	LPIPS ↑	SSIM ↓	PSNR↓	IA ↓
PhotoGuard [77]	201.96	0.68 ± 0.10	0.38 ± 0.09	28.1 ± 0.26	0.79 ± 0.08	103.65	0.35 ± 0.11	0.65 ± 0.10	29.2 ± 0.70	0.90 ± 0.07
AdvDM [49]	255.55	0.69 ± 0.12	0.39 ± 0.05	28.6 ± 0.41	0.78 ± 0.08	109.07	0.40 ± 0.10	0.58 ± 0.08	29.0 ± 0.49	0.89 ± 0.06
Mist [48]	233.71	0.60 ± 0.08	0.42 ± 0.07	28.1 ± 0.25	0.75 ± 0.09	101.25	0.37 ± 0.10	0.62 ± 0.09	29.0 ± 0.62	0.88 ± 0.07
SDS [96]	189.00	0.67 ± 0.12	0.40 ± 0.10	28.2 ± 0.31	0.79 ± 0.08	97.42	0.33 ± 0.09	0.66 ± 0.10	29.4 ± 0.87	0.90 ± 0.06
BlurGuard (Ours)	116.21	0.36 ± 0.11	0.65 ± 0.11	28.5 ± 0.30	0.89 ± 0.06	119.68	0.40 ± 0.10	0.61 ± 0.10	28.4 ± 0.25	0.88 ± 0.06
			JPEG					JPEG + Upsca	aling	
Method	FID ↑	LPIPS ↑	SSIM ↓	PSNR↓	IA ↓	FID ↑	LPIPS ↑	SSIM ↓	PSNR↓	IA ↓
PhotoGuard [77]	141.38	0.51 ± 0.11	0.50 ± 0.07	28.7 ± 0.37	0.85 ± 0.08	105.08	0.36 ± 0.12	0.64 ± 0.09	29.1 ± 0.51	0.88 ± 0.08
AdvDM [49]	217.45	0.59 ± 0.13	0.45 ± 0.06	28.7 ± 0.39	0.83 ± 0.07	130.22	0.36 ± 0.12	0.64 ± 0.09	29.1 ± 0.51	0.88 ± 0.08
Mist [48]	161.10	0.50 ± 0.10	0.50 ± 0.07	28.7 ± 0.36	0.83 ± 0.08	124.02	0.42 ± 0.11	0.59 ± 0.09	28.9 ± 0.42	0.86 ± 0.08
SDS [96]	134.10	0.47 ± 0.11	0.54 ± 0.09	29.1 ± 0.52	0.85 ± 0.08	91.48	0.31 ± 0.09	0.68 ± 0.10	29.7 ± 0.80	0.91 ± 0.06
BlurGuard (Ours)	107.88	0.36 ± 0.10	0.67 ± 0.11	28.5 ± 0.29	0.90 ± 0.05	116.09	0.37 ± 0.10	0.66 ± 0.10	28.4 ± 0.26	0.89 ± 0.06
			DiffPure					GrIDPure	;	
Method	FID ↑	LPIPS ↑	SSIM ↓	PSNR↓	IA ↓	FID ↑	LPIPS ↑	SSIM ↓	PSNR↓	IA ↓
PhotoGuard [77]	92.21	0.35 ± 0.09	0.69 ± 0.12	29.7 ± 1.10	0.92 ± 0.05	128.02	0.34 ± 0.10	0.68 ± 0.12	28.8 ± 0.69	0.88 ± 0.07
AdvDM [49]	98.27	0.37 ± 0.11	0.69 ± 0.11	29.9 ± 1.02	0.91 ± 0.06	123.62	0.40 ± 0.11	0.68 ± 0.08	28.8 ± 0.74	0.89 ± 0.06
Mist [48]	90.96	0.37 ± 0.10	0.69 ± 0.11	29.6 ± 0.85	0.91 ± 0.05	140.20	0.39 ± 0.10	0.64 ± 0.10	28.6 ± 0.71	0.86 ± 0.07
SDS [96]	96.85	0.34 ± 0.09	0.70 ± 0.11	30.1 ± 1.24	0.92 ± 0.05	114.69	0.32 ± 0.09	0.69 ± 0.11	28.7 ± 0.77	0.89 ± 0.07
BlurGuard (Ours)	118.77	0.46 ± 0.10	0.65 ± 0.11	28.5 ± 0.30	0.88 ± 0.06	133.24	0.41 ± 0.10	0.66 ± 0.10	28.5 ± 0.50	0.87 ± 0.06
			Impress					PDM-Pure	e	
Method	FID ↑	LPIPS ↑	SSIM ↓	PSNR↓	IA ↓	FID ↑	LPIPS ↑	SSIM ↓	PSNR↓	IA ↓
PhotoGuard [77]	173.01	0.62 ± 0.10	0.41 ± 0.08	28.2 ± 0.29	0.81 ± 0.08	124.20	0.36 ± 0.10	0.69 ± 0.12	29.6 ± 1.10	0.89 ± 0.06
AdvDM [49]	197.88	0.66 ± 0.10	0.19 ± 0.06	28.4 ± 0.47	0.81 ± 0.08	109.36	0.36 ± 0.11	0.70 ± 0.11	30.0 ± 1.16	0.89 ± 0.06
Mist [48]	209.25	0.63 ± 0.08	0.22 ± 0.09	28.1 ± 0.21	0.77 ± 0.09	121.58	0.38 ± 0.11	0.68 ± 0.12	29.4 ± 0.81	0.88 ± 0.06
SDS [96]	156.37	0.59 ± 0.11	0.44 ± 0.08	28.5 ± 0.35	0.83 ± 0.07	107.19	0.35 ± 0.09	0.69 ± 0.11	30.1 ± 1.20	0.90 ± 0.05
BlurGuard (Ours)	114.12	0.40 ± 0.11	0.60 ± 0.10	28.5 ± 0.27	0.88 ± 0.07	149.44	0.47 ± 0.11	0.64 ± 0.12	28.4 ± 0.29	0.85 ± 0.07

Table 19: Detailed results on image-to-image generation under ℓ_{∞} protection within $\epsilon = \frac{16}{255}$. Before purification represents the protection of the editing result without any purification, while the others show the protection after applying seven different noise purification techniques before editing.

			Before Purific	ation				Noise + Upsca	aling	
Method	FID ↑	LPIPS ↑	SSIM ↓	PSNR↓	IA ↓	FID ↑	LPIPS ↑	SSIM ↓	PSNR↓	IA ↓
PhotoGuard [77]	171.02	0.61 ± 0.08	0.46 ± 0.12	28.4 ± 0.22	0.82 ± 0.08	142.39	0.48 ± 0.11	0.57 ± 0.12	28.8 ± 0.47	0.87 ± 0.08
AdvDM [49]	140.15	0.42 ± 0.12	0.61 ± 0.14	29.6 ± 0.58	0.88 ± 0.08	127.54	0.39 ± 0.11	0.63 ± 0.11	29.2 ± 0.61	0.89 ± 0.08
Mist [48]	131.42	0.44 ± 0.10	0.59 ± 0.10	29.2 ± 0.42	0.88 ± 0.06	124.66	0.39 ± 0.11	0.64 ± 0.12	29.2 ± 0.57	0.89 ± 0.07
SDS [96]	148.46	0.46 ± 0.13	0.60 ± 0.14	29.2 ± 0.69	0.86 ± 0.07	137.87	0.50 ± 0.10	0.56 ± 0.11	28.8 ± 0.42	0.86 ± 0.07
DiffusionGuard [18]	164.81	0.58 ± 0.09	0.50 ± 0.11	28.8 ± 0.33	0.83 ± 0.08	132.70	0.41 ± 0.11	0.62 ± 0.10	29.1 ± 0.51	0.88 ± 0.08
BlurGuard (Ours)	162.92	0.50 ± 0.10	0.59 ± 0.12	28.8 ± 0.59	0.80 ± 0.08	173.90	0.57 ± 0.10	0.52 ± 0.12	28.4 ± 0.25	0.79 ± 0.08
			JPEG					JPEG + Upsca	aling	
Method	FID ↑	LPIPS ↑	SSIM ↓	PSNR↓	IA ↓	FID ↑	LPIPS ↑	SSIM ↓	PSNR↓	IA ↓
PhotoGuard [77]	142.39	0.52 ± 0.10	0.53 ± 0.11	28.9 ± 0.32	0.85 ± 0.08	131.93	0.40 ± 0.11	0.62 ± 0.12	29.2 ± 0.48	0.87 ± 0.08
AdvDM [49]	119.48	0.37 ± 0.14	0.64 ± 0.16	29.7 ± 0.63	0.89 ± 0.08	105.26	0.29 ± 0.11	0.72 ± 0.13	30.0 ± 0.80	0.94 ± 0.05
Mist [48]	118.65	0.38 ± 0.11	0.64 ± 0.13	29.5 ± 0.53	0.90 ± 0.07	109.37	0.31 ± 0.09	0.71 ± 0.08	29.8 ± 0.57	0.92 ± 0.04
SDS [96]	146.17	0.47 ± 0.14	0.57 ± 0.18	29.2 ± 0.64	0.85 ± 0.08	148.93	0.47 ± 0.14	0.54 ± 0.18	29.1 ± 0.55	0.85 ± 0.08
DiffusionGuard [18]	153.17	0.52 ± 0.12	0.52 ± 0.17	29.1 ± 0.45	0.85 ± 0.09	123.32	0.38 ± 0.12	0.65 ± 0.14	29.5 ± 0.57	0.89 ± 0.08
BlurGuard (Ours)	172.08	0.52 ± 0.11	0.56 ± 0.15	28.3 ± 0.28	0.79 ± 0.08	166.08	0.52 ± 0.11	0.56 ± 0.14	28.3 ± 0.25	0.80 ± 0.07
			DiffPure					GrIDPure	;	
Method	FID ↑	LPIPS ↑	SSIM ↓	PSNR↓	IA ↓	FID ↑	LPIPS ↑	SSIM ↓	PSNR↓	IA ↓
PhotoGuard [77]	135.91	0.44 ± 0.12	0.57 ± 0.16	29.0 ± 0.48	0.88 ± 0.07	146.84	0.44 ± 0.12	0.60 ± 0.15	28.5 ± 0.32	0.86 ± 0.08
AdvDM [49]	134.25	0.42 ± 0.11	0.60 ± 0.15	29.2 ± 0.47	0.89 ± 0.08	144.25	0.42 ± 0.12	0.62 ± 0.15	28.5 ± 0.31	0.87 ± 0.08
Mist [48]	129.47	0.41 ± 0.10	0.60 ± 0.13	29.1 ± 0.43	0.90 ± 0.06	142.26	0.40 ± 0.10	0.63 ± 0.12	28.5 ± 0.31	0.88 ± 0.07
SDS [96]	133.78	0.43 ± 0.11	0.59 ± 0.14	29.1 ± 0.41	0.88 ± 0.07	159.96	0.46 ± 0.13	0.57 ± 0.17	28.4 ± 0.30	0.85 ± 0.08
DiffusionGuard [18]	131.03	0.43 ± 0.11	0.59 ± 0.15	29.1 ± 0.42	0.88 ± 0.08	147.91	0.42 ± 0.12	0.61 ± 0.15	28.5 ± 0.31	0.87 ± 0.07
BlurGuard (Ours)	166.29	0.55 ± 0.11	0.52 ± 0.16	28.5 ± 0.28	0.80 ± 0.08	173.50	0.53 ± 0.12	0.56 ± 0.17	28.6 ± 0.35	0.81 ± 0.08
			Impress					PDM-Pur	e	
Method	FID ↑	LPIPS ↑	SSIM ↓	PSNR↓	IA ↓	FID ↑	LPIPS ↑	SSIM ↓	PSNR↓	IA ↓
PhotoGuard [77]	154.18	0.58 ± 0.08	0.47 ± 0.10	28.6 ± 0.23	0.84 ± 0.07	153.37	0.46 ± 0.10	0.61 ± 0.12	29.2 ± 0.46	0.85 ± 0.08
AdvDM [49]	140.84	0.44 ± 0.11	0.59 ± 0.12	29.2 ± 0.40	0.88 ± 0.07	149.97	0.45 ± 0.10	0.60 ± 0.13	29.3 ± 0.50	0.86 ± 0.08
Mist [48]	131.40	0.44 ± 0.10	0.59 ± 0.09	29.1 ± 0.35	0.88 ± 0.06	145.65	0.44 ± 0.11	0.61 ± 0.13	29.3 ± 0.52	0.86 ± 0.08
SDS [96]	154.33	0.48 ± 0.12	0.57 ± 0.14	29.0 ± 0.50	0.85 ± 0.07	156.99	0.45 ± 0.11	0.60 ± 0.13	29.3 ± 0.51	0.85 ± 0.07
DiffusionGuard [18]	161.81	0.57 ± 0.09	0.51 ± 0.10	28.8 ± 0.30	0.84 ± 0.07	149.49	0.46 ± 0.12	0.59 ± 0.15	29.3 ± 0.56	0.86 ± 0.08
BlurGuard (Ours)	168.43	0.51 ± 0.09	0.56 ± 0.10	28.4 ± 0.25	0.80 ± 0.09	180.71	0.57 ± 0.12	0.53 ± 0.16	28.4 ± 0.26	0.79 ± 0.09

Table 20: Detailed results on inpainting under ℓ_{∞} protection within $\epsilon=\frac{16}{255}$. Before purification represents the protection of the editing result without any purification, while the others show the protection after applying seven different noise purification techniques before editing.

			Before Purific	ation				Noise + Upsca	aling	
Method	FID ↑	LPIPS ↑	SSIM ↓	PSNR↓	IA ↓	FID ↑	LPIPS ↑	SSIM ↓	PSNR↓	IA ↓
PhotoGuard [77]	195.57	0.72 ± 0.12	0.20 ± 0.09	28.1 ± 0.30	0.81 ± 0.08	179.01	0.62 ± 0.08	0.22 ± 0.08	28.2 ± 0.27	0.85 ± 0.07
AdvDM [49]	203.50	0.68 ± 0.09	0.16 ± 0.07	28.2 ± 0.39	0.81 ± 0.08	176.74	0.65 ± 0.09	0.17 ± 0.07	28.2 ± 0.26	0.85 ± 0.06
Mist [48]	233.24	0.70 ± 0.08	0.12 ± 0.06	28.2 ± 0.31	0.78 ± 0.08	194.00	0.64 ± 0.09	0.18 ± 0.07	28.2 ± 0.27	0.84 ± 0.07
SDS [96]	203.32	0.69 ± 0.09	0.20 ± 0.08	28.1 ± 0.32	0.82 ± 0.07	176.89	0.61 ± 0.08	0.22 ± 0.08	28.2 ± 0.29	0.87 ± 0.06
BlurGuard (Ours)	190.21	0.64 ± 0.10	0.22 ± 0.10	28.2 ± 0.27	0.82 ± 0.08	181.89	0.63 ± 0.08	0.22 ± 0.10	28.1 ± 0.22	0.83 ± 0.08
			JPEG					JPEG + Upsc	aling	
Method	FID ↑	LPIPS ↑	SSIM ↓	PSNR↓	IA ↓	FID ↑	LPIPS ↑	SSIM ↓	PSNR↓	IA↓
PhotoGuard [77]	180.28	0.64 ± 0.11	0.18 ± 0.07	28.2 ± 0.35	0.86 ± 0.06	177.18	0.61 ± 0.09	0.23 ± 0.09	28.2 ± 0.34	0.86 ± 0.07
AdvDM [49]	188.54	0.67 ± 0.09	0.17 ± 0.06	28.2 ± 0.36	0.82 ± 0.08	188.58	0.66 ± 0.10	0.18 ± 0.07	28.2 ± 0.32	0.84 ± 0.07
Mist [48]	196.23	0.66 ± 0.07	0.14 ± 0.07	28.2 ± 0.33	0.82 ± 0.08	204.39	0.65 ± 0.09	0.15 ± 0.06	28.2 ± 0.32	0.81 ± 0.08
SDS [96]	182.47	0.63 ± 0.09	0.20 ± 0.08	28.2 ± 0.34	0.85 ± 0.06	181.00	0.61 ± 0.09	0.23 ± 0.10	28.2 ± 0.30	0.86 ± 0.06
BlurGuard (Ours)	199.35	0.63 ± 0.09	0.22 ± 0.09	28.1 ± 0.38	0.82 ± 0.07	208.87	0.63 ± 0.08	0.23 ± 0.10	28.1 ± 0.25	0.83 ± 0.07
			DiffPure					GrIDPur	e	
Method	FID ↑	LPIPS ↑	SSIM ↓	PSNR↓	IA ↓	FID ↑	LPIPS ↑	SSIM ↓	PSNR↓	IA ↓
PhotoGuard [77]	200.44	0.67 ± 0.08	0.22 ± 0.10	28.2 ± 0.33	0.84 ± 0.06	196.18	0.63 ± 0.10	0.23 ± 0.10	28.2 ± 0.37	0.84 ± 0.06
AdvDM [49]	194.36	0.70 ± 0.09	0.20 ± 0.09	28.1 ± 0.25	0.82 ± 0.07	204.69	0.64 ± 0.07	0.17 ± 0.07	28.2 ± 0.34	0.83 ± 0.07
Mist [48]	201.93	0.68 ± 0.07	0.20 ± 0.08	28.1 ± 0.23	0.86 ± 0.05	204.09	0.66 ± 0.08	0.17 ± 0.09	28.2 ± 0.28	0.82 ± 0.07
SDS [96]	190.13	0.66 ± 0.07	0.22 ± 0.10	28.2 ± 0.28	0.84 ± 0.06	191.57	0.63 ± 0.09	0.22 ± 0.09	28.2 ± 0.34	0.83 ± 0.09
BlurGuard (Ours)	202.08	0.71 ± 0.07	0.21 ± 0.09	28.0 ± 0.15	0.81 ± 0.08	204.27	0.65 ± 0.10	0.22 ± 0.09	28.1 ± 0.25	0.81 ± 0.07
			Impress					PDM-Pur	e	
Method	FID ↑	LPIPS ↑	SSIM ↓	PSNR↓	IA ↓	FID ↑	LPIPS ↑	SSIM ↓	PSNR↓	IA↓
PhotoGuard [77]	188.37	0.68 ± 0.09	0.19 ± 0.07	28.1 ± 0.19	0.84 ± 0.07	200.25	0.65 ± 0.08	0.23 ± 0.10	28.2 ± 0.40	0.84 ± 0.06
AdvDM [49]	200.67	0.67 ± 0.09	0.17 ± 0.06	28.2 ± 0.29	0.81 ± 0.08	198.20	0.65 ± 0.07	0.20 ± 0.09	28.3 ± 0.39	0.83 ± 0.07
Mist [48]	256.66	0.69 ± 0.08	0.11 ± 0.05	28.2 ± 0.36	0.78 ± 0.08	235.53	0.66 ± 0.11	0.20 ± 0.08	28.2 ± 0.40	0.83 ± 0.06
SDS [96]	181.76	0.66 ± 0.07	0.20 ± 0.07	28.1 ± 0.24	0.84 ± 0.07	189.37	0.65 ± 0.09	0.23 ± 0.10	28.2 ± 0.36	0.84 ± 0.06
BlurGuard (Ours)	202.42	0.64 ± 0.10	0.20 ± 0.08	28.2 ± 0.48	0.81 ± 0.08	221.67	0.69 ± 0.09	0.21 ± 0.08	28.1 ± 0.25	0.81 ± 0.06

Table 21: Detailed results on textual inversion under ℓ_{∞} protection within $\epsilon = \frac{16}{255}$. Before purification represents the protection of the editing result without any purification, while the others show the protection after applying seven different noise purification techniques before editing.